eIF3e and eIF3d control expression of riboproteins and key components of the MAPK signaling pathway.

Anna Herrmannová[1#*], Jan Jelínek[2#], Klára Pospíšilová[1], Farkas Kerényi[1], Tomáš Vomastek[4], Jan Brábek[3], Mahabub Pasha Mohammad[1], Susan Wagner[1], and Leoš Shivaya Valášek[1*]

[1]Laboratory of Regulation of Gene Expression, Institute of Microbiology of the Czech Academy of Sciences, Prague, Videnska 1083, 142 20, the Czech Republic

[2]Laboratory of Bioinformatics, Institute of Microbiology of the Czech Academy of Sciences, Prague, Videnska 1083, 142 20, the Czech Republic

[3]Laboratory of Cancer Cell Invasion, Faculty of Science, Charles University, Prague, Vinicna 7, 128 43, Czech Republic

[4]Laboratory of Cell Signaling, Institute of Microbiology of the Czech Academy of Sciences, Prague, Videnska 1083, 142 20, the Czech Republic

[#] These authors contributed equally to this work.

* To whom the correspondence should be addressed: herrmannova@seznam.cz
valasekl@biomed.cas.cz
Tel: +420 241 062 288
Fax: +420 241 062 665

Running title: eIF3 & signaling and stress transcripts

ABSTRACT

The MAPK cascade plays a key role in transducing extracellular signals into cellular responses. As such, it is unsurprisingly hyperactive in various cancers, primarily due to activating or loss-of-function mutations of its components. Various pathologies, including cancer, are also characterized by deregulated protein synthesis, where imbalanced expression of eIFs is not only a consequence of neoplasia but itself a major contributor to it. eIF3 stands out as the largest, multi-subunit complex with a modular assembly, where aberrant expression of one subunit generates only partially functional subcomplexes. Here, we knocked-down eIF3d, eIF3e and eIF3h in HeLa cells and investigated their impact on differential gene expression by Ribo-Seq. Knock-downs of eIF3d and eIF3e activated the MAPK/ERK1/2 signaling despite reduced protein levels of its multiple components. Depletion of eIF3e and partially eIF3d also increased expression of ribosomal proteins, implicating eIF3 in controlling balanced production of mature ribosomes. Moreover, intact eIF3 also regulates the expression of the proto-oncogene MDM2 and the transcription factor ATF4, both containing short uORFs. eIF3 thus exerts specific translational control over signaling and stress-related transcripts.

Keywords: translation initiation; 40S subunit; eIF3; MAPK; ribosomal protein; differential expression; ribosome profiling

INTRODUCTION

Translational control contributes significantly to the overall regulation of gene expression. Indeed, regulation at the level of translation provides quicker adaptive and usually reversible responses to environmental cues than transcriptional regulation as it acts on pre-existing mRNAs by simply turning their expression on or off (Sonenberg & Hinnebusch, 2009). As such, it critically contributes to the maintenance of overall cellular homeostasis, suggesting that its dysregulation has detrimental effects on cell proliferation and, more broadly, health (Scheper, van der Knaap et al., 2007). In a rapidly growing number of cases, mutations and/or impaired expression of many translational components have been shown to either directly lead to or significantly contribute to various pathological conditions, including cancer (reviewed in (de la Parra, Walters et al., 2018, Robichaud & Sonenberg, 2017, Spilka, Ernst et al., 2013, Sriram, Bohlen et al., 2018)).

Translation can be divided into four stages with the initiation stage playing the most critical role with respect to translational control. It begins with the formation of the 43S pre-initiation complex (PIC) composed of the 40S ribosomal subunit, the eIF2*GTP*Met-tRNA$_i^{Met}$ ternary complex (eIF2-TC), and eIFs 1, 1A, 3, and 5 (reviewed in (Valášek, 2012)). The next step is the mRNA recruitment to form the 48S PIC, which is facilitated by the eIF4F cap-binding complex in concert with eIF3. Once the mRNA is loaded, the 48S PIC starts scanning the mRNA's 5' untranslated region (UTR) until the start codon has been recognized by base-pairing with the Met-tRNA$_i^{Met}$ anticodon. This drives conformational changes in the 48S PIC, co-operatively mediated by eIF1, eIF1A, eIF2, eIF3 and eIF5, resulting in the closure of the 40S mRNA binding channel and subsequent ejection of the eIF2*GDP*eIF5 subcomplex to allow subunit joining to commence (reviewed in (Hinnebusch, 2017)).

Cellular stresses primarily inhibit cap-dependent translation initiation via the eIF4F and eIF2-TC complexes. The former is under the control of two major stress-signaling oncogenic hubs – the anabolic kinase mammalian target of rapamycin complex 1 (mTORC1) and the mitogen-activated protein kinase (MAPK). They promote growth under nutrient-rich and stress-free conditions and deactivate in response to limited supply of amino acids, oxygen, ATP, growth factors or nutrients and play a role in the unfolded protein response (Bhat, Robichaud et al., 2015, Hay & Sonenberg, 2004, Lindqvist, Tandoc et al., 2018). These pathways are hyperactive in the vast majority of cancers, mainly due to activating mutations of RAS, BRAF and PI3K or loss-of-function mutations of the tumor suppressor PTEN, which are among the most common genetic perturbations in cancer (Kandoth, McLellan et al., 2013). The second – eIF2-TC – is a major target of the pro-survival, adaptive pathway called integrated stress response (ISR) encompassing four members of the eIF2α kinase family that respond to a multitude of stimuli including nutrient limitation and endoplasmic reticulum

stress by rapidly shutting down general translation (Pakos-Zebrucka, Koryga et al., 2016).

Mitogen-activated protein kinase (MAPK) cascades have been shown to play a key role in the transduction of extracellular signals into cellular responses. Three families of MAPK signaling pathways have been well characterized in mammalian cells: extracellular signal-regulated kinase (ERK), c-Jun N-terminal kinase/stress-activated protein kinase (JNK/SAPK), and p38 kinase (Zhang & Liu, 2002). The activation of MAPKs is a multistep process. In case of the best described Raf-MEK-ERK pathway, the essential linkers between epidermal growth factor receptors and the MAPK cascade include adaptor protein Grb2, a guanine nucleotide exchange protein Sos, and a small GTP binding protein Ras (Figure 1A). The MAPK cascade begins with MAPKKK (represented by c-Raf) and is followed by MAPKKs such as MEK1 and MEK2. MEKs eventually phosphorylate, and thereby activate p44 MAPK and p42 MAPK, also known as ERK1 and ERK2, respectively (Lavoie, Gagnon et al., 2020, Stokoe, Macdonald et al., 1994). The activated ERKs then translocate to the nucleus where they phosphorylate and transactivate various transcription factors such as c-JUN and c-FOS, thereby altering gene expression to promote growth, differentiation, or mitosis. The ERK/MAPK pathway also directly regulates translational machinery, for example by stimulating the activity of both RSK (Carriere, Ray et al., 2008) and MNK (Buxade, Parra-Palau et al., 2008), with at least the latter pathway also responding to agonists of the p38 MAPK pathway. MNK interacts with eIF4G and upon activation phosphorylates eIF4E at Ser209, a site that increases the oncogenic potential of eIF4E and facilitates translation of specific mRNAs related to migration, metastasis and inflammation (Pyronnet, Imataka et al., 1999). Following the stimulation of the ERK pathway, activated RSK phosphorylates rpS6, eIF4B, eEF2K, and PDCD4, which are all important translational regulators (reviewed in (Bhat et al., 2015, Robichaud & Sonenberg, 2017)). RSK also participates in the regulation of mTORC1 by inhibiting TSC2 (Roux, Ballif et al., 2004) and Deptor (Zhao, Xiong et al., 2011); both are negative regulators of mTORC1. ERK and RSK regulate LKB1-dependent and -independent phosphorylation of Raptor (Carriere, Cargnello et al., 2008), resulting in increased mTORC1 signaling. In addition, ERK and RSK also co-operate to regulate ribosome biogenesis by promoting TIF-1A phosphorylation (reviewed in (Roux & Topisirovic, 2018)).

It has been shown that alterations in genomic sequences, levels, stoichiometry, and/or activity of eIFs and other components of the translational apparatus and relevant signaling cascades, as well as in cis-regulatory elements of mRNAs, can circumvent the stress-induced translational shutdown that these pathways impose by allowing selective recruitment of mRNAs, rewiring translational control of mRNA cis-regulatory elements, and/or enabling alternative start codon selection (Ruggero, 2013, Sriram et al., 2018). Naturally, this leads to various pathologies. Overexpression of eIF4F complex

components, for example, has been observed in various cancer entities (Bhat et al., 2015, De Benedetti & Harris, 1999, Ruggero, 2013, Shuda, Kondoh et al., 2000, Truitt & Ruggero, 2016). In addition to eIF4F components, dysregulation of the multi-subunit eIF3 complex is also involved in oncogenesis. Ten of the twelve eIF3 subunits have been linked to human cancers, many due to overexpression (a, b, c, d, g, h, m or i), some due to underexpression (e and f) (reviewed in (de la Parra et al., 2018, Gomes-Duarte, Lacerda et al., 2018, Hershey, 2015, Valasek, Zeman et al., 2017, Zhang, Pan et al., 2007)). In addition, some eIF3 subunits have been shown to directly interact with certain pathology-related mRNAs (Lee, Kranzusch et al., 2015), and very recently, it has been proposed that the eIF3k subunit serves as a regulator of cancer-relevant ribosome content (Duan, Zhang et al., 2023). Despite all these observations, the exact mechanism(s) by which eIF3 affects various pathologies is virtually unknown. Moreover, many studies that address the effect of eIF3 in specific diseases focus on only one subunit of eIF3 and neglect the need to consider their findings in the context of the entire eIF3.

Here, we call attention to this unfortunate trend. eIF3 is the largest and most complex eIF of all eIFs, it is modular in nature (Figure 1B) (reviewed in (Cate, 2017, Valasek et al., 2017, Wolf, Lin et al., 2020)), and plays multiple roles not only in translation initiation, but also in termination, ribosomal recycling and stop codon readthrough (Beznosková, Cuchalová et al., 2013, Beznoskova, Wagner et al., 2015, Pisarev, Hellen et al., 2007, Poncova, Wagner et al., 2019). Each of these roles may be regulated differently by individual subunits and/or their combinations, making it practically impossible to study them in isolation. Eight eIF3 subunits (a, c, e, f, h, k, l and m) form a structural scaffold called the PCI (**P**roteasome, **C**OP9, e**I**F3) / MPN (**M**pr1-**P**ad1 **N**-terminal) octamer, whereas the remaining four non-octameric subunits (b, d, g and i) are likely to be more flexible. The essential subunits b, g, and i form a separate module that is connected to the octamer *via* the C-terminal domain (CTD) of eIF3a; together they are called YLC for **Y**east **L**ike **C**ore (Wagner, Herrmannova et al., 2016). The eIF3d subunit is located on the eIF3 periphery and is attached to the octamer primarily via eIF3e, but partly also *via* eIF3a and c (Bochler, Querido et al., 2020, Brito Querido, Sokabe et al., 2020). On the 40S subunit, the octamer is positioned close to the mRNA exit site, whereas the mobile YLC shuffles between the mRNA entry site and the subunit interface during the AUG selection process (des Georges, Dhote et al., 2015, Llacer, Hussain et al., 2021, Llácer, Hussain et al., 2018, Simonetti, Guca et al., 2020).

We recently reported a comprehensive *in vivo* analysis of the modular dynamics of the human eIF3 complex (Wagner, Herrmannova et al., 2020, Wagner, Herrmannova et al., 2014, Wagner et al., 2016). Using a systematic individual downregulation strategy, we showed that the expression of all 12 eIF3 subunits is interconnected such that perturbance of the expression of one subunit results in the down-regulation of entire

modules leading to the formation of partial eIF3 subcomplexes with limited functionality (Herrmannova, Prilepskaja et al., 2020). Here we took advantage of this knowledge to examine the specific effect of selected eIF3 subcomplexes on the translation efficiency translatome-wide in HeLa cells.

MATERIALS AND METHODS

Whole cell extract (WCE) preparation and transfection

HeLa cells were grown at 37 °C and 5% CO2 in Ø 15 cm dishes in DMEM (Sigma, cat #D6429) supplemented with 10% FBS (Gibco, cat # 10270-106). Twenty-four hours after seeding, cells were transfected with the ON-TARGETplus siRNA cocktail system from Dharmacon at a final concentration of 5 nM. Catalog numbers for all siRNAs used in this study are listed in Supplementary Table S1. INTERFERin (Polyplus, cat # 101000016) was used as a transfection reagent, 100 µl per dish. Cells were harvested 72 hours after transfection, as described previously (Herrmannova et al., 2020) at approximately 80% confluency.

Ribosome profiling (Ribo-Seq) and RNA-seq library preparation

For **footprint (FP) libraries** cycloheximide was added to a final concentration of 100 µg/ml 1 min prior to harvesting. Cells were washed with ice cold 1x PBS and lysed in buffer A (10 mM HEPES [pH 7.5], 62.5 mM KCl, 2.5 mM $MgCl_2$, 1 mM DTT, 1 mM PMSF, 1 µg/ml Aprotinin, 1 µg/ml Leupeptin, 1 µg/ml Pepstatin, Complete Mini EDTA-free [Roche, cat # 11836170001] – 1 tablet/5 ml, 1% Triton X-100, 100 µg/ml Cycloheximide) on the dish. The resulting lysate was collected and cleared by centrifugation. Aliquots of twelve absorbance units (AU) OD_{260} of WCE were flash frozen in liquid nitrogen and used for control polysome profile and footprint isolation. An aliquot of 1 mg total protein was taken for control western blot, and another 200 µl aliquot was mixed with 1 ml of RNA Blue (TopBio, cat # R013) and taken for RNA isolation and control qPCR. When the lysate passed all three control experiments (polysome profile, western blot, qPCR), one aliquot of 12 AU OD_{260} was thawed on ice, digested with 5 µl RNAseI (Ambion, cat # AM2295) for 30 min at 24 °C with mild shaking (300 rpm) and inactivated with SuperaseIN (Ambion, cat #AM2696). 80S ribosomes were separated by high-velocity sedimentation through a 5% to 45% sucrose gradient at 39,000 rpm for 2.5 h using the SW41Ti rotor. The gradients were scanned at 254 nm to visualize the ribosomal species and fractions containing 80S ribosomes were collected and mixed with RNA Blue. RNA was isolated according to vendor's instructions, FP RNA was size selected on 15% TBE-Urea PAGE (Biorad, cat # 3540092) in range 20-40 nt and footprint library was prepared according to (Ingolia, Brar et al., 2012). FP libraries were sequenced on NovaSeq6000 (Illumina) with read length 50 nt.

For **mRNA libraries** the growth media was aspirated and cells were harvested into 5 ml of RNA Blue per Ø 15 cm dish. RNA was isolated according to vendor's instructions. mRNA was isolated from the total RNA using Poly(A)purist MAG kit (Ambion, cat # AM1922), fragmented using RNA Fragmentation Reagents (Ambion, cat # AM8740) and size selected on 15% TBE-Urea PAGE in range 50-100 nt. Size

selected mRNA was then dephosphorylated and library was prepared using SMARTer smRNA-Seq Kit (TAKARA, cat # 635029) according to vendor's instructions. mRNA libraries were sequenced on NovaSeq6000 (Illumina) with read length 150 nt.

RNA isolation, reverse transcription and qPCR

Total RNA was isolated using RNA Blue reagent (TopBio, cat # R013) 72 h post-transfection according to the manufacturer's instructions. After DNase I digestion (NEB, cat # M0303L), cDNA was synthesized from 1µg RNA using the High-Capacity cDNA Reverse Transcription Kit (Applied Biosystems, # 4368813). qPCR was performed in triplicates using 5× HOT FIREPol EvaGreen qPCR Mix Plus (Solis BioDyne # 08-25-00020). The obtained data were normalized to ALAS1 mRNA levels and non-transfected control. All qPCR primers are listed in Supplementary Table S2.

Western blotting

All samples were resolved using SDS-PAGE followed by western blotting. All primary antibodies used in this study are listed in Supplementary Table S3. The signal was developed using SuperSignal West Femto Maximum Sensitivity Substrate (Thermo Scientific, cat # 34096) and detected in a G-Box imager (Syngene) using a series of varying exposure times.

Polysome profiles

One aliquot of 12 AU OD_{260} was thawed on ice and separated by high-velocity sedimentation through a 5% to 45% sucrose gradient at 39,000 rpm for 2.5 h using the SW41Ti rotor. The gradients were scanned at 254 nm to visualize the ribosomal species.

Analysis of Sequencing Data

We processed the ribosome **footprint libraries** as follows. Adapter sequence "CTGTAGGCACCATCAAT" and all sequences 3' of the adapter were trimmed from the 3' end of each read by Cutadapt v. 3.5 (Martin, 2011). Flanking Ns were trimmed from both 5' and 3' ends of each read. Reads without adapter sequence and reads shorter than 15 nt after trimming were discarded. Next, rRNA and tRNA reads were discarded after alignment with Bowtie2 v. 2.4.4 (Langmead & Salzberg, 2012). For rRNA, we used RNA5S1, RNA5-8SN5, RNA18SN5 and RNA28SN5 from NCBI (Sayers, Bolton et al., 2022), and ENSG00000211459 and ENSG00000210082 from Ensembl (Howe, Achuthan et al., 2021). For tRNA we used all human tRNA sequences from tRNAdb (Juhling, Morl et al., 2009) and all high confidence hg38 tRNA sequences from GtRNAdb (Chan & Lowe, 2016). Remaining reads were aligned to genome and transcriptome from Ensembl (GRCh38.p13, annotation release 104) by the STAR aligner v. 2.7.9a_2021-06-25 (Dobin, Davis et al., 2013) using local alignment with 10%

mismatches, and with indels and soft clipping allowed for transcriptomic alignment. Gene counts were counted from genomic alignment using Samtools index v. 1.13 (Danecek, Bonfield et al., 2021) and Htseq-count v. 0.13.5 (Anders, Pyl et al., 2015) within CDS regions. Transcriptomic alignments were further processed using MANE Select set from MANE project v. 0.95 (Morales, Pujar et al., 2022) and custom programs "mane2ensembl_gtf", "filter_reverse_reads", "filter_ambiguous_genes" and "select_transcripts". See Supplementary Spreadsheet S1 for detailed overview of raw read processing.

The RNA-seq libraries were processed the same as above, except that raw read processing by Cutadapt had to be adapted to different library construction method (SMARTer smRNA-Seq Kit, TAKARA). In particular, first 3 nucleotides on the 5' end were removed, and poly(A) sequence (10xA) was trimmed from the 3'end.

Quality checks were done by FastQC v. 0.11.9 (Andrews, 2010) and Ribo-seQC v. 1.1 (Calviello, WSydow et al., 2019). Triplet periodicity was checked on transcriptomic alignments using custom modified riboWaltz (Lauria, Tebaldi et al., 2018) and a custom script "Triplet_periodicity.R". Gene counts were used to check correlation between replicates using a custom script "Correlation-samples.R". Read length counts were used to check read length distribution using a custom script "Lengths.R".

PCA plot, sample distances clustering and the differential expression analysis were performed on gene counts by DESeq2 (Love, Huber et al., 2014) with biomaRt library (Durinck, Spellman et al., 2009) used to download gene annotations. Differential TE values between NT and the knock-downs were calculated as described in (Chothani, Adami et al., 2019). The p_{adj} threshold for differentially translated transcripts was set to 0.05. For details see custom script "Differential analysis.R". Results of differential expression analysis were further used to generate heatmap and scatterplots of differentially expressed genes and genes with defined p-adjusted value were used to analyze dependency between mRNA characteristics and changes in TE using custom scripts "Significant_TE_heatmap.R", "Significant_TE_intersection.R" and "Correlation-features.R". To get mRNA characteristics we used MANE Select set to select a single representative transcript for each protein-coding gene. uORF database uORFdb (Manske, Ogoniak et al., 2023) was used to get number of ATG uORFs per mRNA. For metagene analysis, custom programs "transcripts_startstop_positions", "read_counts" and "region_readcounts" were used to get read counts relative to the start codon. These were normalized to a number of reads in a region starting 75 bases after the start codon and ending 15 bases before the stop codon and averaged over the samples. Only transcripts that met the following parameters were considered: CDS longer than 450 nt, at least 128 raw counts (or 64 normalized counts), and RPKM higher than 10. Moving average method was used with a 21 bases window size. All used custom scripts are available on Github.

We analyzed enrichment of the differentially translated transcripts in KEGG pathways (Kanehisa & Sato, 2020) and Gene Ontology (Ashburner, Ball et al., 2000, Gene Ontology, 2021) using Enrichr (Kuleshov, Jones et al., 2016), ShinyGO v0.741 (Ge, Jung et al., 2020) and KEGG Mapper Search (Kanehisa, Sato et al., 2022). Venn diagrams were created using InteractiVenn (Heberle, Meirelles et al., 2015).

RESULTS

High quality sequencing libraries prepared from HeLa cells expressing different eIF3 subcomplexes.

To investigate the impact of different human eIF3 subunits and partial eIF3 sub-complexes, which arise in cells as a result of unbalanced eIF3 expression, on translational efficiency translatome-wide, we performed Ribo-Seq together with RNA-Seq, which allowed us to draw conclusions about gene expression at the transcriptional and translational levels and their interdependence. In particular, using the siRNA technology, we examined HeLa cells with reduced levels of eIF3d, eIF3e or eIF3h subunits and cells treated with non-targeting (NT) siRNA. While eIF3d downregulation leads to a reduction in protein levels of only eIF3d and leaves the rest of the eIF3 complex intact, downregulation of eIF3e or eIF3h generates partial eIF3 subcomplexes as previously described (Wagner et al., 2016). Specifically, targeting eIF3e with siRNA results in reduced protein levels of eIF3e, eIF3d, eIF3k and eIF3l, whereas downregulation of eIF3h produces a partial eIF3 complex lacking subunits eIF3h, eIF3k and eIF3l (Figure 1B). In terms of impact on cell growth, both eIF3d^{KD} and eIF3e^{KD} display strongly reduced proliferation, while the effect of eIF3h^{KD} is only moderate (Wagner et al., 2016).

We first performed several control experiments with aliquots of cell lysates made to prepare individual Ribo-Seq libraries to document an efficient downregulation of the targeted eIF3 subunit, as well as the expected phenotype (Wagner et al., 2016). Using qPCR, we measured mRNA levels of the siRNA targeted eIF3 subunits (eIF3d, eIF3e, eIF3h), as well as eIF3b as a negative control and a housekeeping gene ALAS1 for normalization purposes. Routinely, a difference of 4 to 5 cycles was achieved for each downregulated subunit, corresponding to ~16–32 fold decrease in its mRNA level; the mRNA levels of the control subunit eIF3b remained unchanged (Figure 2A); note that Figure 2A summarizes qPCR results for all samples used to generate of Ribo-Seq and RNA-Seq libraries.

Next, we checked protein levels of selected eIF3 subunits by Western blotting (Figure 2B). Protein levels of all eIF3 subunits targeted individually by siRNA showed a visible drop; in the case of eIF3e^{KD}, a marked decrease in the eIF3d protein level was also evident, as previously reported (Wagner et al., 2016). Finally, we performed polysome profiling to assess the impact on translation and obtained essentially the same results as before (Supplementary Figure 1A) (Wagner et al., 2016). The eIF3d^{KD}

showed the most pronounced defect in translation initiation, marked by a robust increase of the 80S monosome peak and a concomitant decrease of polysome content, similar to eIF3e^{KD}, while eIF3h^{KD} had only a modest effect.

Ribo-Seq libraries were generated from each knock-down and NT control in three biological replicates as described in (Ingolia et al., 2012). RNA-Seq libraries were prepared in four biological replicates using the SMARTer smRNA-Seq Kit to normalize for mRNA levels and calculate translational efficiency (TE). Both Ribo-Seq and RNA-seq libraries were highly reproducible as shown by the Spearman correlation coefficient (Supplementary Figure 1B). All Ribo-Seq libraries showed a similar read length distribution with a prominent peak at 30 – 32 nt and an expected 3 nt periodicity in coding sequences (CDS) (Supplementary Figure 2A and Figure 2C). As expected, Ribo-seq libraries were strongly enriched for CDS reads compared to RNA-Seq libraries (Supplementary Figure 2B – C). The PCA plot and hierarchical clustering (Figure 3A and Supplementary Figure 3A) showed clustering of the samples into two main groups: Ribo-Seq and RNA-seq, and also into two subgroups; NT and eIF3h^{KD} samples clustered on one side and eIF3e^{KD} and eIF3d^{KD} samples on the other, reflecting their similar impact on translational efficiency translatome-wide, as shown below.

eIF3 subcomplexes alter translation efficiency of a large proportion of genes

Using the R DESeq2 package (Love et al., 2014), we identified transcripts with significantly altered TE ($P_{adjusted} < 0.05$) for each knock-down compared to the NT control (Figure 3B – D, Supplementary Spreadsheet S2), henceforth referred to as Differential Translation Efficiency Genes (DTEGs) (Chothani et al., 2019). In total, we identified 21 DTEGs in eIF3h^{KD} (19 downregulated and 2 upregulated), 1180 DTEGs in eIF3e^{KD} (622 down and 558 up), and 1971 DTEGs in eIF3d^{KD} (1040 down and 931 up) out of a total of 17520 genes that were assigned TE values.

The number of DTEGs in each knock-down correlated well with the severity of the overall phenotype and with the impact on global translation, as shown in the polysome profiles (Supplementary Figure 1A). eIF3d^{KD} with the strongest decrease in polysomes had the highest number of DTEGs, whereas eIF3h^{KD} with only 21 DTEGs had a marginal effect on the amount of polysomes. Similarly, the overall distribution of changes in the TE-fold showed most pronounced changes in eIF3d^{KD} (Supplementary Figure 3B). It should be noted, however, that in contrast to polysome profiling, differential expression analysis of Ribo-Seq data normalizes out global changes in translational rates, and reveals only specific shifts of ribosome localization on individual mRNAs between the NT and KD datasets. In agreement, all three knock-downs showed an increase in TE for approximately half of the affected genes, reflecting specific regulation rather than simply non-specific global translation shutdown.

Interestingly, there is a considerable overlap between the knock-downs studied, such that only 1045 DTEGs are unique for eIF3d^{KD} and the rest (926) are shared with

other two knock-downs; in particular 923 with eIF3e^{KD} and 21 with eIF3h^{KD} – in the latter case, the overlap reaches 100% (Figure 3E, Supplementary Figure 3C – E). Remarkably, eIF3d^{KD} affects neither the expression of any other eIF3 subunit nor the integrity of the eIF3 complex, yet it has the most pronounced impact on translation (Wagner et al., 2016), correlating well with the highest number of DTEGs identified. In case of eIF3e^{KD}, only 257 DTEGs are unique and the rest (923) are shared with eIF3d^{KD}, 18 of which are also shared with eIF3h^{KD} (Figure 3E, Supplementary Figure 3C – E). The eIF3 subcomplex formed in eIF3e^{KD} lacks subunits e, k and l and partially also eIF3d (Wagner et al., 2016) – the significantly reduced protein levels of eIF3d are evident in Figure 2B. Thus, it is not surprising that the DTEGs identified in eIF3e^{KD} largely overlap with those identified in eIF3d^{KD}; in fact, this result supports the robustness and accuracy of this approach. The fact that the magnitude of the knock-down effect is bigger in eIF3d^{KD} over eIF3e^{KD} is discussed below.

eIF3d^{KD} and eIF3e^{KD} decrease translation efficiency of the key components of the MAPK/ERK and other signaling pathways implicated in cancer

To analyze enrichment in KEGG pathways and GO Biological Processes in a meaningful way, we analyzed the DTEGs divided not only into downregulated and upregulated groups, but also into specific subgroups – eIF3d^{KD} "all", eIF3e^{KD} "all", eIF3d^{KD} "unique", eIF3e^{KD} "unique" and eIF3d^{KD}/eIF3e^{KD} "common" (Figure 3E – G). To disentangle the effects of transcriptional and translational regulation, we also investigated translationally exclusive DTEGs whose mRNA abundance did not change significantly and therefore the change in TE can be attributed solely to translational regulation; eIF3d^{KD} "translation only" and eIF3e^{KD} "translation only" (see further below).

The eIF3d^{KD} or eIF3e^{KD} "all downregulated" and eIF3d^{KD}/eIF3e^{KD} "common downregulated" groups were enriched for a similar set of KEGG pathways (Figure 4A and Supplementary Figure 4). The effect is generally stronger for eIF3d^{KD}, which simply means that this knock-down has a higher number of DTEGs in the same pathway than eIF3e^{KD} (for example MAPK signaling pathway: 42 vs. 30 DTEGs for eIF3d^{KD} vs. eIF3e^{KD}, respectively). Therefore, we focused primarily on DTEGs identified in eIF3d^{KD} "all" (Figure 4A and Supplementary Figure 4). Most of the top ten KEGG results are related to and/or encompass the MAPK signaling pathway (Supplementary Figure 5A), like Chronic myeloid leukemia and the Neurotrophin signaling pathway. The MAPK signaling pathway, which plays a critical role in the regulation of cell proliferation (Zhang & Liu, 2002) and unsurprisingly in cancer development and progression (reviewed in (Dhillon, Hagan et al., 2007)), has been affected at all levels, starting with the docking protein Grb2 (encoded by *GRB2*) and guanine nucleotide exchange factor Sos (*SOS1*), through kinases c-Raf (*RAF1*), MEK1 (*MAP2K1*), Erk2 (*MAPK1*), MNK1 (*MKNK1*), Rsk2 (*RPS6KA3*), to the transcription factor CREB (*ATF4*). In addition, PAK1, that activates c-Raf, was also significantly affected (Figure 1A, Supplementary Figure 5B and

Supplementary Spreadsheet S2). Consistently, Gene Ontology (GO) analysis revealed strong association of downregulated DTEGs with biological processes "protein phosphorylation" and "regulation of transcription" and the molecular function term "protein serine/threonine kinase activity" (Supplementary Figure 6A – B). Key integrin-mediated signaling proteins that were implicated in cancer cell plasticity, adhesion, migration and survival (reviewed in (Cooper & Giancotti, 2019)) also had significantly decreased TE, specifically, proto-oncogenes Crk (*CRK*) and Crk-L (*CRKL*), *PRKCA* – a catalytic subunit of PI3-kinase, Rac1 GTPase (*RAC1*), JNK2 (*MAPK9*), as well as Abl1 kinase (*ABL1*) and BCR activator of Rho-GEF (*BCR*). The TGF-beta signaling, important for a wide range of cellular processes as well as for tumor cell invasion, metastasis, and resistance to chemotherapy (reviewed in (Colak & Ten Dijke, 2017)), was affected at the level of the intracellular transducer Smad4 (*SMAD4*) and receptor activated SMADs, namely Smad3 (*SMAD3*) and Smad5 (*SMAD5*) and TGF beta (*TGFB3*) itself. The NFkB pathway, a regulator of immune and inflammatory responses (Liu, Zhang et al., 2017), also implicated in cancer cell proliferation, survival, angiogenesis and plasticity (reviewed in (Xia, Shen et al., 2014)), was downregulated at the level of NFkB (*NFKB1*) itself and IKK kinase (*CHUK*). Notably, a direct link between activation of NFkB and eIF3 has very recently been described (She, Luo et al., 2023). Finally, the canonical Wnt signaling pathway, which shapes the stem cells-like properties of cancer cells and boosts proliferation (reviewed in (Zhang & Wang, 2020)), was downregulated at the level of a protein Dishevelled (*DVL3*) and GSK3 beta kinase (*GSK3B*). For the complete list of all DTEGs, please see Supplementary Spreadsheet S2.

eIF3d^{KD} and eIF3e^{KD} reduce protein levels of key components of the activated MAPK/ERK pathway.

Interestingly, 26 of the 42 downregulated DTEGs belonging to the MAPK signaling pathway can be classified as translationally buffered; i.e., their mRNA levels increase while their TE decreases (Kusnadi, Timpone et al., 2022). However, this is a somewhat unusual case of translational buffering because transcriptional upregulation is not only nullified by translational repression, but completely overruled, so that the total number of FPs is also reduced. To verify that the reduction in TE and FP counts is indeed manifested by a reduction in cellular protein levels, we selected a set of genes with different combinations of changes in TE or FP or mRNA levels, including translationally exclusive and translationally buffered genes, as well as genes with unchanged TE, and subjected them to western blotting (Figure 4B - C).

We found, that AKT1, GRB2, MAP2K1 (MEK1), RPS6KA1 (RSK1), RPS6KA3 (RSK2), RAF1 and SOS1 had visibly decreased protein levels in eIF3d^{KD} and some of them also in eIF3e^{KD}. The only exception, which showed no changes in protein levels, was PAK1, which Ribo-seq data suggested to have decreased TE, FP counts, as well

as mRNA levels. This discrepancy could be explained by the non-specificity of the available polyclonal antibody that cross-react with PAK1-related proteins PAK2 and PAK3. Another interesting exception is the transcription factor c-Jun, which showed increased mRNA and FP levels, unchanged TE, but robust increases in protein levels in all three knock-downs (Figure 4C). The mRNA levels of all selected genes were verified by qPCR, showing a good correlation with our sequencing data; whereas PAK1 showed significant decrease, c-JUN mRNA was significantly increased in both eIF3d^{KD} and eIF3e^{KD} (Supplementary Figure 6C). To assess the functional consequences of the downregulation of MAPK pathway components, we examined the phosphorylation status of downstream kinases ERK1/2, which directly phosphorylate several transcription factors including c-JUN (Leppa, Saffrich et al., 1998). As with other MAPK proteins, ERK1/2 expression was reduced in eIF3d^{KD} and eIF3e^{KD}, but its phosphorylation at Thr202/Tyr204 was clearly increased in all three knock-downs (Figure 4D). Thus, despite reduced MAPK pathway protein levels, MAPK signaling appears to be activated when eIF3 function in translation is compromised.

eIF3d^{KD} specifically reduces TE of components of the PI3K-Akt signaling pathway, while eIF3e contributes to genotoxic stress prevention

DTEGs that were downregulated only in eIF3d^{KD} but not in other KDs (eIF3d^{KD} "unique downregulated" DTEGs; 545 in total) showed specific enrichment in the inositol phosphate metabolism and phosphatidylinositol signaling KEGG pathways and GO terms primarily associated with genes involved in transcription regulation (Supplementary Figure 6D - E). The phosphatidylinositol signaling pathway was affected at the level of phosphoinositide production. Several kinases mediating phosphorylation of phosphatidylinositol (*PIK3C2A*, *PIK3CA*, *PIP4K2A*, *IPMK* and *ITPK1*) showed a significant decrease in TE. Phosphoinositides are involved in many signaling pathways, such as the PI3K-Akt pathway that mediates cell proliferation, survival, and metabolism (Balla, 2013).

The eIF3e^{KD} "unique downregulated" DTEGs (129 in total) were mostly enriched in KEGG pathways of homologous recombination and transcriptional misregulation in cancer and in related GO terms, such as double-strand break repair via synthesis-dependent strand annealing, telomere maintenance, histone acetylation or import into nucleus (Supplementary Figure 6F-G), all, when deregulated, causing genotoxic stress that may drive cells to apoptosis. Interestingly, eIF3e contains a bipartite nuclear localization sequence (NLS) and a putative N-terminal nuclear export signal (NES) (Guo & Sen, 2000). Therefore, eIF3e could potentially shuttle between the nucleus and the cytoplasm to modulate transcription in the nucleus.

eIF3d^{KD} and eIF3e^{KD} increase TE of proteins associated with membrane organelles

Analysis of DTEGs upregulated in eIF3d^{KD} and eIF3e^{KD} showed similar results for almost all groups analyzed (eIF3d^{KD} "all", "unique", and "translation only", eIF3d^{KD}/eIF3e^{KD} "common", as well as eIF3e^{KD} "all" and "translation only") (Figure 5A, B, and Supplementary Figure 7), with the strongest enrichment in the KEGG "Lysosome" and "Protein processing in endoplasmic reticulum" pathways. The majority of DTEGs in these pathways were solely translationally regulated meaning that their mRNA levels stayed unchanged while the TE increased. For example, for the KEGG pathway "Lysosome", more than 70%, precisely 37 out of the 51 DTEGs upregulated in the eIF3d^{KD} "all", fall into the eIF3d^{KD} "translation only" group. This suggests that when translation initiation is compromised by eIF3d/e^{KD}, cells increase protein degradation and turnover by translationally upregulating lysosomal and ER proteins. Interestingly and in accord with our results, Lin et al. detected increased lysosomal load in MCF-10A cells downregulated for eIF3e (Lin, Li et al., 2020). They speculated that this is due to the need to clear defective mitochondria. In support, we found enrichment of mitochondria-associated DTEGs, especially mitochondrial ribosomal proteins (see below).

As for the eIF3d^{KD} "unique upregulated" DTEGs, we identified one interesting and unique KEGG pathway, the ABC transporters (Supplementary Figure 7, in green). A total of 12 different ABC transporters had elevated TE (9 of them are unique to eIF3d^{KD}, while 3 were also found in eIF3e^{KD}), 6 of which (ABCC1-5, ABCC10) belong to the C subfamily, known to confer multidrug resistance with alternative designation as multidrug resistance protein (MRP1-5, MRP7) (Sodani, Patel et al., 2012). Interestingly, all six of these ABCC transporters were upregulated solely on the translational level (Supplementary Spreadsheet S2).

eIF3e^{KD} increases production of ribosomal proteins

Interestingly, the KEGG pathway "Ribosome" and GO terms connected with translation and ribosome biogenesis were enriched amongst DTEGs upregulated specifically in eIF3e^{KD} "unique upregulated" DTEGs (Figure 5C and Supplementary Figure 8A). We then compared the significance of enrichment for Ribosome term between eIF3e^{KD} and eIF3d^{KD} "all upregulated" groups. This was the only case where a term or a pathway was more significantly enriched in eIF3e^{KD} (P = 5.199E-10) than in eIF3d^{KD} (NS, P = 0.1183) (Supplementary Figure 7, in green). Intrigued by this result, we filtered out all ribosomal proteins (RPs) from our data set (according to HGNC database, (Tweedie, Braschi et al., 2021)), regardless of the TE changes, which consisted of 89 cytoplasmic and 77 mitochondrial RPs, and analyzed them separately (Supplementary Spreadsheet S2). In total, we identified 32 RPs with significantly changed TE in eIF3e^{KD} (14 cytoplasmic and 18 mitochondrial) and only 16 in eIF3d^{KD} (9 cytoplasmic and 7 mitochondrial). Moreover, all the cytoplasmic RPs with increased TE in eIF3e^{KD} (and most mitochondrial ones) were upregulated solely on the translational level and their

mRNA levels were not changed. We selected several RPs with different combinations of changes in TE or FP or mRNA levels in both eIF3e^{KD} and eIF3d^{KD} (Figure 5D) and subjected them to western blotting. All ribosomal proteins tested showed visibly increased protein levels in both eIF3e^{KD} and eIF3d^{KD} (Figure 5E), while their mRNA levels remained unchanged (Supplementary Figure 8B). For some RPs (RPS2, RPS3), the increase was more pronounced in eIF3e^{KD}. Overall, our results suggest that eIF3e and, to some extent, its binding partner eIF3d positively control RPs production in the cell. Interestingly, an antagonistic role has recently been attributed to eIF3k, which has been shown to specifically repress the synthesis of the small ribosomal protein RPS15A (Duan et al., 2023). Noteworthy, targeting eIF3e with siRNA results in co-downregulation of not only eIF3e and eIF3d, but also of eIF3k and eIF3l (Wagner et al., 2016).

In addition to mitochondrial RPs, we also observed increased TE for several other mitochondrial proteins from the Complex I, Complex IV and Complex V (KEGG term Oxidative phosphorylation hsa00190; rank 17; #of genes 12 out of 134; p = 0.0003431) in eIF3e^{KD}, but many of these transcripts, mainly from the Complex I, are translated in mitochondria directly, so these results should be verified by Mitoribosome profiling, as the traditional Ribo-Seq method is not suitable for this (Pearce, Cipullo et al., 2021).

Intact eIF3 contributes to translational regulation of ATF4 and MDM2

Knocking down eIF3h generates an eIF3 subcomplex lacking eIF3h and two nonessential subunits eIF3k and eIF3l (Figure 1B), having only negligible impact on overall translation. Accordingly, we identified 19 transcripts whose TE was decreased and only 2 transcripts whose TE was increased compared to the NT control (Figure 3E - G). Given the low number of DTEGs, we observed no significant enrichment of any KEGG pathway within the upregulated DTEGs and only a few significant enrichments for the eIF3h^{KD} “all downregulated” DTEGs in pathways like Prostate cancer, Viral carcinogenesis or PI3-Akt signaling pathway, all of which included only two common hits – MDM2 and ATF4 (Figure 6A, Supplementary Table S4). Additionally, we also noticed enrichment of GO terms associated with ubiquitination (Figure 6B, Supplementary Table S5), which was mainly due to the MDM2, WAC, RNF10, RMND5A, USP38 and ZRANB1 genes, all of which showed a decrease in TE. Note that all of the above downregulated DTEGs are common for all three knock-downs.

Perhaps the most interesting of these genes is the proto-oncogene MDM2, an E3 ubiquitin ligase acting as a negative regulator of the p53 protein (Marine & Lozano, 2010), whose overexpression has been reported in many different cancer types (Rayburn, Zhang et al., 2005). We did confirm that the MDM2 protein levels were reduced in all three knock-downs (Figure 6C). Of note, the WAC protein is also an E3 ubiquitin ligase associated with p53 regulation because it forms a complex with RNF20

and RNF40, which together directly interact with p53 (Meng, Guo et al., 2021). RMND5A and RNF10 are also the E3 ubiquitin ligases. RMND5A is a member of the CTLH complex that regulates expression of Raf1 proto-oncogene and promotes cell migration and adhesion (Chen, Chen et al., 2021), while RNF10 targets 40S ribosomes for degradation upon ribosome stalling and has also been proposed as a prognostic marker for renal clear cell carcinoma and hepatocellular carcinoma (Gao, Ye et al., 2021, Zhu, Li et al., 2021). Importantly, all these ubiquitin ligases are downregulated exclusively on the translational level.

In contrast, USP38 and ZRANB1 are de-ubiquitinases. ZRANB1 is implicated in cancer by regulating EZH2 – the catalytic component of the polycomb repressive complex 2 (PRC2), and USP38 is involved in regulating the stability of oncoprotein c-Myc (Xu, Hu et al., 2021, Zhang, Xiao et al., 2018).

An equally interesting DTEG like MDM2 is ATF4, which is among the top 10 most significant DTEGs in all three knock-downs (Figure 3B - D). In eIF3h^{KD}, it can be classified as a translationally buffered gene because it has strongly upregulated mRNA levels, but this increase is not accompanied by a concomitant increase in the FP count, thereby resulting in decreased TE. In eIF3d^{KD} and eIF3e^{KD}, it is even significantly translationally repressed (FPs are decreased). Using qPCR, we confirmed its transcriptional upregulation in all three knock-downs (Supplementary Figure 8C). Because ATF4 protein levels are on the verge of the western blot detection limit under non stress condition, we examined whether all three knock-downs tested had any effect on ATF4 induction upon 3 hour-long ER stress provoked by 1mM Thapsigargin (Harding, Novoa et al., 2000). Indeed, stress-mediated ATF4 induction was almost abolished in eIF3d^{KD} and eIF3e^{KD} and strongly decreased in eIF3h^{KD} (Figure 6D). This differential effect correlates nicely with our sequencing data, where the decrease in TE was also stronger in eIF3d^{KD} and eIF3e^{KD}. ATF4 protein levels in DMSO control are shown as a no stress reference. Overall, these findings further confirm that an intact eIF3 complex is required for proper translational control of ATF4, as we and others have previously suggested (Guan, van Hoef et al., 2017, Hronova, Mohammad et al., 2017, Shu, Mao et al., 2022, Wagner, Bohlen et al., 2022), and as discussed below.

Presence of uORFs, UTR length and GC content correlate with the change in translation efficiency

eIF3 is critically required for mRNA recruitment to the 40S ribosomal subunit (reviewed in (Valasek et al., 2017)) and several eIF3 subunits have been proposed to regulate translation of specific subsets of mRNAs (Lee et al., 2015, Lee, Kranzusch et al., 2016). We therefore asked whether the changes in TE that we observed in the eIF3d, eIF3e or eIF3h knock-downs correlate with certain mRNA properties. Indeed, in all three knock-downs, the change in TE was negatively correlated with the length of 5' and 3' UTR (Spearman correlation, $P < 1x10^{-45}$). Moreover, we found a significant positive

Spearman correlation between TE changes and the GC content in the coding region (CDS) and 3' UTRs (Figure 7A).

To explore these correlations in more detail, we focused only on those mRNAs that are exclusively regulated at the translational level in each knock-down and therefore should contain distinct features that facilitate their translational regulation. We divided them into those with significantly changed TE (decreased and increased) and those with unchanged TE and searched for significant differences in the median values of the tested traits (Figure 7B - C). In accordance with the Spearman correlation, in eIF3d^{KD} and eIF3e^{KD}, mRNAs of downregulated DTEGs had longer 5' UTRs, while upregulated DTEGs possessed shorter 5' UTRs, when compared to mRNAs with unchanged TE. The same trend is seen for the 3' UTR length in eIF3e^{KD}, but with lower significance. In case of eIF3d^{KD}, only the downregulated DTEGs showed a significant change in 3' UTR length, but not DTEGs that were upregulated.

In terms of GC content, while we observed little significant difference in GC content in the 5' UTR of eIF3d^{KD} and eIF3e^{KD}, there was a highly significant difference in the CDS and 3' UTR of these knock-downs in both downregulated and upregulated DTEGs, indicating that mRNAs with increased TE tend to have more GC-rich 3' UTRs and, surprisingly, CDS and vice versa. For eIF3h^{KD}, we only observed differences of low significance due to the low number of DTEGs that were only translationally regulated (only 8 downregulated and 1 upregulated) (data not shown).

In summary, mRNAs with decreased TE in cells downregulated for eIF3d and eIF3e have on average longer 5' and 3' UTRs and lower GC content in the CDS and 3' UTRs, whereas mRNAs with increased TE have on average shorter 5' UTRs and a higher GC content in the CDS and 3' UTRs.

We next asked whether 5' UTRs of upregulated or downregulated DTEGs contain any specific sequence motifs or short upstream open reading frames (uORFs) that would explain the observed differences. We did not identify any specific sequence motif, but we did note that TE changes show a significant negative correlation with the amount of uORFs (Figure 7A). Moreover, the 5' UTRs of "downregulated translation only" DTEGs have a strong tendency to contain uORFs starting with AUG (Figure 7D - E). These findings suggest that the intact eIF3 complex is primarily required for efficient translation of mRNAs containing short uORFs in their 5' UTR, like for example MDM2 and ATF4, which is in line with its role in translation reinitiation (reviewed in (Valasek et al., 2017)), and further discussed below.

DISCUSSION

In this study, we subjected three eIF3 subunits to siRNA-mediated depletion in HeLa cells followed by RNA-Seq and Ribo-Seq to elucidate their role in translational regulation of specific mRNAs by differential expression analysis. We focused on

differential translation efficiency genes (DTEGs) and identified several interesting groups of DTEGs associated with individual eIF3 knock-downs.

Interestingly, while DTEGs identified in eIF3d^{KD} and eIF3e^{KD} largely overlapped, considerably more DTEGs were identified in eIF3d^{KD} then in eIF3e^{KD}, correlating well with the severity of the growth phenotype of both knock-downs, with the former being more detrimental despite having zero effect on eIF3 integrity apart from lacking eIF3d subunit (Wagner et al., 2016). The higher number of DTEGs identified in the same pathways in eIF3d^{KD} vs. eIF3e^{KD} could be explained by differences in eIF3d protein levels between the two knock-downs. Despite being markedly downregulated also in eIF3e^{KD}, it is still more highly expressed then in eIF3d^{KD}, where it is directly targeted by siRNA, whereas in eIF3e^{KD} its downregulation is only a secondary effect. Further, eIF3d is a peripheral subunit that binds to the head of the 40S subunit (mainly via the small ribosomal protein Rps16 (Herrmannova et al., 2020)) and is connected to the eIF3 octamer not only via eIF3e but also via the eIF3a and c subunits (Bochler et al., 2020). Therefore, we hypothesize that eIF3d may remain partially operational even in the absence of eIF3e, and therefore the more severe phenotype in eIF3d^{KD} is mainly due to lower levels of eIF3d compared to eIF3e^{KD}. Following this logic, phenotypes that are common to eIF3d^{KD} and eIF3e^{KD} are likely a consequence of a lack of eIF3d protein.

Perhaps the most intriguing finding is that eIF3d^{KD} and, to a large extent, also eIF3e^{KD} result in translational repression of a marked number of the MAPK pathway constituents, which significantly reduces their protein levels, despite the cell's apparent compensatory efforts to increase their transcription. Somewhat unexpectedly, the largely downregulated MAPK pathway is activated as evidenced by elevated ERK1/2 phosphorylation. Notably, the eIF3d influence on the MAPK pathway was previously demonstrated in HTR-8/SVneo cells, where overexpression of eIF3d led to hypo-phosphorylation of MEK1 and ERK1/2, while downregulation had the opposite effect; however, no significant effect on the protein levels of its components was detected in this study (Li, Wang et al., 2021). Importantly, since the increased ERK1/2 phosphorylation was observed not only in eIF3d^{KD} and eIF3e^{KD} but also in eIF3h^{KD}, where expression of MAPK pathway proteins is unaffected, we conclude that activation of the MAPK pathway is a general consequence of compromised eIF3 function. Perhaps intracellular MAPK sensing is so sensitive that even a subtle interference with the eIF3 function suffices to trigger its activation.

Expression of the transcription factor c-Jun is partially controlled by the activated MAPK pathway and, consistently, we found that it is strongly upregulated in all three knock-downs. Interestingly, c-Jun was previously shown to interact directly with eIF3 through a stable stem loop occurring in its 5' UTR, which positively stimulates its translation (Lee et al., 2015). However, in our case the upregulation occurred only on transcriptional level and the impaired function of eIF3 had no effect on its translational efficiency. Nonetheless, considering that eIF3 function is impaired in our knock-downs,

the mere c-Jun transcriptional upregulation can be explained as an indirect compensatory measure to boost protein levels of c-Jun in cells with compromised translation. Because c-Jun is a component of the AP1 transcription factor and either homodimerizes or heterodimerizes with other AP1 proteins, we examined mRNA, FP and TE trends of other AP1 factors in our data. Only FOSL1 and ATF3 showed increased mRNA levels and FP counts with no net changes in TE like c-Jun, whereas other members of the JUN family (JUNB and JUND) and FOS family (FOS, FOSB, FOSL2) remained unchanged, and the ATF family members ATF2 and ATF4 were even downregulated. Further research is needed to unravel the full spectrum of changes associated with the activated MAPK pathway in eIF3-impaired cells.

Recently, Lin et al. carried out a similar analysis in MCF-10A cells downregulated for eIF3e (Lin et al., 2020). Naturally, we cross-referenced our data with their eIF3e^{KD}-specific DTEGs (240 downregulated and 220 upregulated) and eIF3e-dependent mRNAs. They identified a set of 2683 eIF3e-dependent mRNAs encoding many proteins associated with mitochondrial and membrane functions that showed increased ribosome density between codons 25 and 75 in eIF3e^{KD}. Those mRNAs were therefore proposed to require eIF3e to recruit chaperons to promote their early elongation. However, we did not observe a similar phenomenon in our datasets. In metagene analysis, we did observe some accumulation of footprints at the beginning of the CDS, but this was present in all samples, including NT, and peaked already around codon 20 after the start codon (Supplementary Figure 8D). In any case, if Lin et al. are correct, it opens an important issue. Such an “accumulation effect”, resulting from ribosome stalling or slower elongation/termination rates, could artificially increase FPs and TE without actually increasing the expression of the proteins so affected. To ensure that this was not the case, we trimmed the first 225 nt (75 codons) from all mRNA’s CDSs, and repeated the differential expression analysis. When compared, the two DE analyses showed approximately 80% - 90% identical DTEGs and high correlation (Spearman correlation coefficient of eIF3d^{KD}: 0.924, eIF3e^{KD}: 0.925, eIF3h^{KD}: 0.834), suggesting that our DE analysis is not biased by ribosome accumulation in the first 75 codons and reflects true changes in translation efficiency. Interestingly, comparing our DTEGs with the Lin et al. data, we found a very significant overlap of 446 genes between the eIF3e-dependent mRNAs and our eIF3d^{KD} “all upregulated” set of mRNAs ($P < 1x10^{-53}$), while the overlap with eIF3e^{KD} “all upregulated” – 251 genes – was surprisingly smaller ($P < 1x10^{-24}$). Moreover, our KEGG enrichment analysis of eIF3e-dependent mRNAs from Lin et al. revealed the same top 2 KEGG pathways (data not shown) as in case of eIF3d^{KD} “all upregulated” group; i.e. Lysosome and Protein processing in ER (Figure 5A, B and Supplementary Figure 7). Considering that eIF3d was naturally co-depleted with eIF3e in the eIF3e^{KD} of Lin et al., it is quite possible, if their model is correct, that not eIF3e but the eIF3d subunit (or cooperatively both

subunits together) ensures loading of quality control factors to promote elongation of transmembrane proteins. In any case, resolving this issue will require further research.

In fact, based on our analysis, eIF3e could be instead involved in controlling the balanced production of mature ribosomes, as its loss resulted in significant number of "unique upregulated" DTEGs with strong enrichment for the KEGG Ribosome and GO Translation and Ribosome biogenesis terms (Figure 5C and Supplementary Figure 8A). Focusing directly on RPs, nearly twice as many RPs with significantly altered TEs were identified in eIF3e^{KD} compared to eIF3d^{KD} (32 vs. 16) and a similar pattern was also evident at the FP level (91 vs. 64). Interestingly, despite this obvious difference, RPs were increased similarly in both eIF3d^{KD} and eIF3e^{KD} (Figure 5E). Therefore, it seems likely that both eIF3 subunits contribute to this regulatory mechanism and that the effect of translational upregulation is amplified when they are simultaneously depleted. The observed discrepancy between the Ribo-Seq and Western blot results in eIF3e^{KD} *versus* eIF3d^{KD} (Figure 5D *vs.* 5E) can be explained by the enhanced stabilization of RPs by the previously described compensatory dosage mechanism at the protein level (Ishikawa, 2021). In particular, to preserve the stoichiometry of the ribosome when numerous RPs are translationally upregulated, the rest of the RPs would be protected from degradation. This speculation can be supported by the impact of all knock-downs on translation efficiency of different E3 ubiquitin ligases, as described for eIF3h^{KD} (Supplementary Table S5).

Interestingly, all cytoplasmic RPs with increased TE in eIF3e^{KD} (and most of mitochondrial RPs) were upregulated solely on translational level (their mRNA levels did not change). It is well-known that RP mRNAs belong to the TOP mRNAs family. They contain a polypyrimidine tract in their 5' UTR and seem to be regulated translationally in response to stress or unfavorable growth conditions (Cockman, Anderson et al., 2020). Besides RPs, this family also includes some translational initiation and elongation factors. Upregulation of cytosolic ribosomal proteins has previously been reported in association with the eIF3m downregulation – albeit only at transcriptional level (Smekalova, Gerashchenko et al., 2020), or with downregulation of eEF2 (Gerashchenko, Nesterchuk et al., 2020). One of the identified regulators stimulating 5' TOP mRNAs translation is LARP1 (Tcherkezian, Cargnello et al., 2014). However, our data suggests that LARP1 protein production was unchanged as the FP count was not altered. Yet translation of TOP mRNAs was strongly upregulated. Nonetheless, it has been reported that the LARP1-dependent control of TOP mRNAs expression is only one of many proposed mechanisms (Meyuhas & Kahan, 2015). What actually causes the observed specific increase in RPs expression in eIF3e^{KD} is currently under investigation in our laboratory.

In addition, as we were unable to find any specific sequence motif in the 5' UTR's of the knock-down affected mRNAs, we cross-referenced our eIF3d^{KD} "all" and eIF3e^{KD} "all" groups with transcripts that physically interact with eIF3, probably by a distinct

secondary structures, as reported by (Lee et al., 2015). We found that of the 402 transcripts with a putative but in most cases unverified binding site for eIF3 in their 5' UTRs, 92 and 65 had significantly altered TE in the eIF3d^{KD} and eIF3e^{KD}, respectively (51 were common for both eIF3d^{KD} and eIF3e^{KD}) (Figure 7F). This notable overlap involving for example MAPK1 gene further underscores the robustness of our screening approach.

Among the few downregulated DTEGs in eIF3h^{KD}, we found two intriguing hits in *ATF4* and *MDM2* mRNAs, whose translation is tightly regulated by the presence of uORFs in their 5' UTRs in response to specific stress conditions (Akulich, Sinitcyn et al., 2019, Dey, Baird et al., 2010). In fact, both mRNAs were translationally downregulated in all three knock-downs. The fact that transcripts of both of these genes contain uORFs in their 5' UTRs also correlates well with our finding that 5' UTRs of "downregulated translation only" DTEGs have a strong tendency to contain AUG-initiated uORFs (Figure 7D, E). Noteworthy, the impaired *ATF4* induction under ER stress, as demonstrated here, has been reported before for knock-downs of several eIF3 subunits (eIF3a, eIF3c, eIF3d, eIF3g, but not eIF3l) (Guan et al., 2017). Moreover, eIF3h and specifically modified eIF3a have been directly shown to modulate resumption of scanning from *ATF4*'s uORF1 for efficient reinitiation downstream; i.e. one of the key steps in the *ATF4* translational control (Hronova et al., 2017, Shu et al., 2022). Therefore, we propose that the entire intact eIF3 complex is required for stimulation of reinitiation on uORF-containing mRNAs, such as *ATF4* and *MDM2*, to ensure their efficient translation on demand. Interestingly, the impact on translation of *MDM2* mRNA could indicate that intact eIF3 also contributes to the metabolism the key tumor suppressor p53 (Marine & Lozano, 2010), which is the focus of our further research.

Among the few DTEGs in eIF3h^{KD}, only MUC2 and PRRC2A were upregulated. The latter was significantly upregulated in all three knock-downs and was recently identified by the Teleman's group as a protein interacting with the translational machinery, including eIF3. Interestingly, they found that PRRC2 proteins affected translation initiation by promoting leaky scanning (Bohlen, Roiuk et al., 2023) and the triple knock-down of all PRRC2 proteins (PRRC2A, PRRC2B, PRRC2C) specifically decreased translation efficiency of mRNAs harboring uORFs in their 5' UTRs, similar to our eIF3 knock-downs. Thus, we speculate that by increased expression of PRRC2A (and also PRRC2B and PRRC2C in eIF3d^{KD} and eIF3e^{KD}), cells attempt to compensate for ineffective translation of mRNAs with uORFs, which often encode regulatory proteins. Indeed, there are several mRNAs with uORFs that are downregulated in both our and Teleman's data sets, such as MAPKAP1 or RAF1. Intriguingly, all PRRC2 proteins themselves have a highly translated overlapping-uORF in their 5' UTR, suggesting that they are subject to an autoregulatory mechanism.

Although our results presented here and summarized in Figure 7G are limited to HeLa cells and future work is required to confirm their universal validity in other cells

and tissues, growing evidence suggests that eIF3 plays a critical role in translational regulation of specific mRNAs encoding regulatory proteins, very often making use of uORFs and/or specific secondary structures in their 5' UTRs (Lee et al., 2015). A great number of these proteins has been implicated in oncogenic signaling and tumor progression, and therefore many of them are considered actionable target for drug development. Since malignant cells exhibit augmented activity of many components of the translation machinery and are inherently believed to become "addicted" to elevated protein synthesis (Ruggero, 2013, Silvera, Formenti et al., 2010), it is increasingly apparent that targeting directly general components of the canonical translational machinery, such as eIF3, which act virtually upstream of effector proteins directly involved in tumorigenesis, may hold promise for overcoming the major obstacle associated with intratumor heterogeneity.

SUPPLEMENTARY DATA

Supplementary Data are available at NAR online.

DATA AVAILABILITY

The datasets generated during this study were deposited in the GEO database with the following accession number: GSE216967. All custom programs source code are published at https://github.com/cas-bioinf/RibosomeProfiling.

ACKNOWLEDGMENTS

We are thankful to Olga Krýdová for technical and administrative assistance and to all lab members for fruitful discussions. We are also thankful to Jonathan Bohlen for sharing and discussing results of PRRC2 proteins downregulation.

FUNDING

This work was supported by a Grant of Excellence in Basic Research (EXPRO 2019) provided by the Czech Science Foundation (19-25821X to L.S.V.), Czech Science Foundation grant 19-08013S (to T.V), ELIXIR CZ research infrastructure project (MEYS Grant No: LM2023055) including access to computing and storage facilities, and by National Institute for Cancer Research (Programme EXCELES, ID Project No. LX22NPO5102) funded by the European Union - Next Generation EU (to J.B.).

CONFLICT OF INTEREST

The authors declare no competing interests.

REFERENCES

Akulich KA, Sinitcyn PG, Makeeva DS, Andreev DE, Terenin IM, Anisimova AS, Shatsky IN, Dmitriev SE (2019) A novel uORF-based regulatory mechanism controls

translation of the human MDM2 and eIF2D mRNAs during stress. Biochimie 157: 92-101
Anders S, Pyl PT, Huber W (2015) HTSeq--a Python framework to work with high-throughput sequencing data. Bioinformatics 31: 166-9
Andrews S (2010) FastQC: A quality control tool for high throughput sequence data. .
Ashburner M, Ball CA, Blake JA, Botstein D, Butler H, Cherry JM, Davis AP, Dolinski K, Dwight SS, Eppig JT, Harris MA, Hill DP, Issel-Tarver L, Kasarskis A, Lewis S, Matese JC, Richardson JE, Ringwald M, Rubin GM, Sherlock G (2000) Gene ontology: tool for the unification of biology. The Gene Ontology Consortium. Nat Genet 25: 25-9
Balla T (2013) Phosphoinositides: tiny lipids with giant impact on cell regulation. Physiol Rev 93: 1019-137
Beznosková P, Cuchalová L, Wagner S, Shoemaker CJ, Gunišová S, Von der Haar T, Valášek LS (2013) Translation initiation factors eIF3 and HCR1 control translation termination and stop codon read-through in yeast cells. PLoS Genet 9: e1003962
Beznoskova P, Wagner S, Jansen ME, von der Haar T, Valasek LS (2015) Translation initiation factor eIF3 promotes programmed stop codon readthrough. Nucleic Acids Res 43: 5099-111
Bhat M, Robichaud N, Hulea L, Sonenberg N, Pelletier J, Topisirovic I (2015) Targeting the translation machinery in cancer. Nat Rev Drug Discov 14: 261-78
Blankenberg D, Von Kuster G, Bouvier E, Baker D, Afgan E, Stoler N, Galaxy T, Taylor J, Nekrutenko A (2014) Dissemination of scientific software with Galaxy ToolShed. Genome Biol 15: 403
Bochler A, Querido JB, Prilepskaja T, Soufari H, Simonetti A, Del Cistia ML, Kuhn L, Ribeiro AR, Valasek LS, Hashem Y (2020) Structural Differences in Translation Initiation between Pathogenic Trypanosomatids and Their Mammalian Hosts. Cell Rep 33: 108534
Bohlen J, Roiuk M, Neff M, Teleman AA (2023) PRRC2 proteins impact translation initiation by promoting leaky scanning. Nucleic Acids Res 51: 3391-3409
Brito Querido J, Sokabe M, Kraatz S, Gordiyenko Y, Skehel JM, Fraser CS, Ramakrishnan V (2020) Structure of a human 48S translational initiation complex. Science 369: 1220-1227
Buxade M, Parra-Palau JL, Proud CG (2008) The Mnks: MAP kinase-interacting kinases (MAP kinase signal-integrating kinases). Front Biosci 13: 5359-73
Calviello L, WSydow D, Harnett D, Ohler U (2019) Ribo-seQC: comprehensive analysis of cytoplasmic and organellar ribosome profiling data. bioRxiv 601468
Carriere A, Cargnello M, Julien LA, Gao H, Bonneil E, Thibault P, Roux PP (2008) Oncogenic MAPK signaling stimulates mTORC1 activity by promoting RSK-mediated raptor phosphorylation. Curr Biol 18: 1269-77
Carriere A, Ray H, Blenis J, Roux PP (2008) The RSK factors of activating the Ras/MAPK signaling cascade. Front Biosci 13: 4258-75

Cate JH (2017) Human eIF3: from 'blobology' to biological insight. Philos Trans R Soc Lond B Biol Sci 372
Chan PP, Lowe TM (2016) GtRNAdb 2.0: an expanded database of transfer RNA genes identified in complete and draft genomes. Nucleic Acids Res 44: D184-9
Chen S, Chen Y, Wen Y, Cai W, Zhu P, Yuan W, Li Y, Fan X, Wan Y, Li F, Zhuang J, Jiang Z, Wu X, Wang Y (2021) miR-590-5p targets RMND5A and promotes migration in pancreatic adenocarcinoma cell lines. Oncol Lett 22: 532
Chothani S, Adami E, Ouyang JF, Viswanathan S, Hubner N, Cook SA, Schafer S, Rackham OJL (2019) deltaTE: Detection of Translationally Regulated Genes by Integrative Analysis of Ribo-seq and RNA-seq Data. Curr Protoc Mol Biol 129: e108
Cockman E, Anderson P, Ivanov P (2020) TOP mRNPs: Molecular Mechanisms and Principles of Regulation. Biomolecules 10
Colak S, Ten Dijke P (2017) Targeting TGF-beta Signaling in Cancer. Trends Cancer 3: 56-71
Cooper J, Giancotti FG (2019) Integrin Signaling in Cancer: Mechanotransduction, Stemness, Epithelial Plasticity, and Therapeutic Resistance. Cancer Cell 35: 347-367
Danecek P, Bonfield JK, Liddle J, Marshall J, Ohan V, Pollard MO, Whitwham A, Keane T, McCarthy SA, Davies RM, Li H (2021) Twelve years of SAMtools and BCFtools. Gigascience 10
De Benedetti A, Harris AL (1999) eIF4E expression in tumors: its possible role in progression of malignancies. Int J Biochem Cell Biol 31: 59-72
de la Parra C, Walters BA, Geter P, Schneider RJ (2018) Translation initiation factors and their relevance in cancer. Curr Opin Genet Dev 48: 82-88
des Georges A, Dhote V, Kuhn L, Hellen CU, Pestova TV, Frank J, Hashem Y (2015) Structure of mammalian eIF3 in the context of the 43S preinitiation complex. Nature 525: 491-5
Dey S, Baird TD, Zhou D, Palam LR, Spandau DF, Wek RC (2010) Both transcriptional regulation and translational control of ATF4 are central to the integrated stress response. J Biol Chem 285: 33165-74
Dhillon AS, Hagan S, Rath O, Kolch W (2007) MAP kinase signalling pathways in cancer. Oncogene 26: 3279-90
Dobin A, Davis CA, Schlesinger F, Drenkow J, Zaleski C, Jha S, Batut P, Chaisson M, Gingeras TR (2013) STAR: ultrafast universal RNA-seq aligner. Bioinformatics 29: 15-21
Duan H, Zhang S, Zarai Y, Ollinger R, Wu Y, Sun L, Hu C, He Y, Tian G, Rad R, Kong X, Cheng Y, Tuller T, Wolf DA (2023) eIF3 mRNA selectivity profiling reveals eIF3k as a cancer-relevant regulator of ribosome content. EMBO J: e112362
Durinck S, Spellman PT, Birney E, Huber W (2009) Mapping identifiers for the integration of genomic datasets with the R/Bioconductor package biomaRt. Nat Protoc 4: 1184-91

Gao J, Ye F, Han F, Wang X, Jiang H, Zhang J (2021) A Novel Radiogenomics Biomarker Based on Hypoxic-Gene Subset: Accurate Survival and Prognostic Prediction of Renal Clear Cell Carcinoma. Front Oncol 11: 739815
Ge SX, Jung D, Yao R (2020) ShinyGO: a graphical gene-set enrichment tool for animals and plants. Bioinformatics 36: 2628-2629
Gene Ontology C (2021) The Gene Ontology resource: enriching a GOld mine. Nucleic Acids Res 49: D325-D334
Gerashchenko MV, Nesterchuk MV, Smekalova EM, Paulo JA, Kowalski PS, Akulich KA, Bogorad R, Dmitriev SE, Gygi S, Zatsepin T, Anderson DG, Gladyshev VN, Koteliansky VE (2020) Translation elongation factor 2 depletion by siRNA in mouse liver leads to mTOR-independent translational upregulation of ribosomal protein genes. Sci Rep 10: 15473
Gomes-Duarte A, Lacerda R, Menezes J, Romao L (2018) eIF3: a factor for human health and disease. RNA Biol 15: 26-34
Guan BJ, van Hoef V, Jobava R, Elroy-Stein O, Valasek LS, Cargnello M, Gao XH, Krokowski D, Merrick WC, Kimball SR, Komar AA, Koromilas AE, Wynshaw-Boris A, Topisirovic I, Larsson O, Hatzoglou M (2017) A Unique ISR Program Determines Cellular Responses to Chronic Stress. Mol Cell 68: 885-900 e6
Guo J, Sen GC (2000) Characterization of the interaction between the interferon-induced protein P56 and the Int6 protein encoded by a locus of insertion of the mouse mammary tumor virus. J Virol 74: 1892-1899
Harding HP, Novoa I, Zhang Y, Zeng H, Wek R, Schapira M, Ron D (2000) Regulated translation initiation controls stress-induced gene expression in mammalian cells. Mol Cell 6: 1099-1108
Hay N, Sonenberg N (2004) Upstream and downstream of mTOR. Genes Dev 18: 1926-45
Heberle H, Meirelles GV, da Silva FR, Telles GP, Minghim R (2015) InteractiVenn: a web-based tool for the analysis of sets through Venn diagrams. BMC Bioinformatics 16: 169
Herrmannova A, Prilepskaja T, Wagner S, Sikrova D, Zeman J, Poncova K, Valasek LS (2020) Adapted formaldehyde gradient cross-linking protocol implicates human eIF3d and eIF3c, k and l subunits in the 43S and 48S pre-initiation complex assembly, respectively. Nucleic Acids Res 48: 1969-1984
Hershey JW (2015) The role of eIF3 and its individual subunits in cancer. Biochim Biophys Acta 1849: 792-800
Hinnebusch AG (2017) Structural Insights into the Mechanism of Scanning and Start Codon Recognition in Eukaryotic Translation Initiation. Trends Biochem Sci 42: 589-611
Howe KL, Achuthan P, Allen J, Allen J, Alvarez-Jarreta J, Amode MR, Armean IM, Azov AG, Bennett R, Bhai J, Billis K, Boddu S, Charkhchi M, Cummins C, Da Rin Fioretto L,

Davidson C, Dodiya K, El Houdaigui B, Fatima R, Gall A et al. (2021) Ensembl 2021. Nucleic Acids Res 49: D884-D891
Hronova V, Mohammad MP, Wagner S, Panek J, Gunisova S, Zeman J, Poncova K, Valasek LS (2017) Does eIF3 promote reinitiation after translation of short upstream ORFs also in mammalian cells? RNA biol: doi: 10.1080/15476286.2017.1353863
Ingolia NT, Brar GA, Rouskin S, McGeachy AM, Weissman JS (2012) The ribosome profiling strategy for monitoring translation in vivo by deep sequencing of ribosome-protected mRNA fragments. Nat Protoc 7: 1534-50
Ishikawa K (2021) Multilayered regulation of proteome stoichiometry. Curr Genet 67: 883-890
Juhling F, Morl M, Hartmann RK, Sprinzl M, Stadler PF, Putz J (2009) tRNAdb 2009: compilation of tRNA sequences and tRNA genes. Nucleic Acids Res 37: D159-62
Kandoth C, McLellan MD, Vandin F, Ye K, Niu B, Lu C, Xie M, Zhang Q, McMichael JF, Wyczalkowski MA, Leiserson MDM, Miller CA, Welch JS, Walter MJ, Wendl MC, Ley TJ, Wilson RK, Raphael BJ, Ding L (2013) Mutational landscape and significance across 12 major cancer types. Nature 502: 333-339
Kanehisa M, Sato Y (2020) KEGG Mapper for inferring cellular functions from protein sequences. Protein Sci 29: 28-35
Kanehisa M, Sato Y, Kawashima M (2022) KEGG mapping tools for uncovering hidden features in biological data. Protein Sci 31: 47-53
Kuleshov MV, Jones MR, Rouillard AD, Fernandez NF, Duan Q, Wang Z, Koplev S, Jenkins SL, Jagodnik KM, Lachmann A, McDermott MG, Monteiro CD, Gundersen GW, Ma'ayan A (2016) Enrichr: a comprehensive gene set enrichment analysis web server 2016 update. Nucleic Acids Res 44: W90-7
Kusnadi EP, Timpone C, Topisirovic I, Larsson O, Furic L (2022) Regulation of gene expression via translational buffering. Biochim Biophys Acta Mol Cell Res 1869: 119140
Langmead B, Salzberg SL (2012) Fast gapped-read alignment with Bowtie 2. Nat Methods 9: 357-9
Lauria F, Tebaldi T, Bernabo P, Groen EJN, Gillingwater TH, Viero G (2018) riboWaltz: Optimization of ribosome P-site positioning in ribosome profiling data. PLoS Comput Biol 14: e1006169
Lavoie H, Gagnon J, Therrien M (2020) ERK signalling: a master regulator of cell behaviour, life and fate. Nat Rev Mol Cell Biol 21: 607-632
Lee AS, Kranzusch PJ, Cate JH (2015) eIF3 targets cell-proliferation messenger RNAs for translational activation or repression. Nature 522: 111-4
Lee AS, Kranzusch PJ, Doudna JA, Cate JH (2016) eIF3d is an mRNA cap-binding protein that is required for specialized translation initiation. Nature 536: 96-99
Leppa S, Saffrich R, Ansorge W, Bohmann D (1998) Differential regulation of c-Jun by ERK and JNK during PC12 cell differentiation. EMBO J 17: 4404-13

Li X, Wang Z, Liu G, Guo J (2021) EIF3D promotes the progression of preeclampsia by inhibiting of MAPK/ERK1/2 pathway. Reprod Toxicol 105: 166-174
Lin Y, Li F, Huang L, Polte C, Duan H, Fang J, Sun L, Xing X, Tian G, Cheng Y, Ignatova Z, Yang X, Wolf DA (2020) eIF3 Associates with 80S Ribosomes to Promote Translation Elongation, Mitochondrial Homeostasis, and Muscle Health. Mol Cell 79: 575-587 e7
Lindqvist LM, Tandoc K, Topisirovic I, Furic L (2018) Cross-talk between protein synthesis, energy metabolism and autophagy in cancer. Curr Opin Genet Dev 48: 104-111
Liu T, Zhang L, Joo D, Sun SC (2017) NF-kappaB signaling in inflammation. Signal Transduct Target Ther 2: 17023-
Llacer JL, Hussain T, Dong J, Villamayor L, Gordiyenko Y, Hinnebusch AG (2021) Large-scale movement of eIF3 domains during translation initiation modulate start codon selection. Nucleic Acids Res 49: 11491-11511
Llácer JL, Hussain T, Gordiyenko Y, Lorsch JR, Hinnebusch AG, Ramakrishnan V (2018) The beta propellers of eIF3b and eIF3i relocate together to the ribosomal intersubunit interface during translation initiation. bioRxiv: 453688
Love MI, Huber W, Anders S (2014) Moderated estimation of fold change and dispersion for RNA-seq data with DESeq2. Genome Biol 15: 550
Manske F, Ogoniak L, Jurgens L, Grundmann N, Makalowski W, Wethmar K (2023) The new uORFdb: integrating literature, sequence, and variation data in a central hub for uORF research. Nucleic Acids Res 51: D328-D336
Marine JC, Lozano G (2010) Mdm2-mediated ubiquitylation: p53 and beyond. Cell Death Differ 17: 93-102
Martin M (2011) Cutadapt removes adapter sequences from high-throughput sequencing reads. EMBnetjournal 17: 10-12
Meng D, Guo K, Zhang D, Zhao C, Sun C, Zhang F (2021) Ring finger 20/ring finger 40/WW domain-containing adaptor with coiled-coil complex interacts with p53 to regulate gene transcription in DNA damage response. Oncol Lett 21: 436
Meyuhas O, Kahan T (2015) The race to decipher the top secrets of TOP mRNAs. Biochim Biophys Acta 1849: 801-11
Morales J, Pujar S, Loveland JE, Astashyn A, Bennett R, Berry A, Cox E, Davidson C, Ermolaeva O, Farrell CM, Fatima R, Gil L, Goldfarb T, Gonzalez JM, Haddad D, Hardy M, Hunt T, Jackson J, Joardar VS, Kay M et al. (2022) A joint NCBI and EMBL-EBI transcript set for clinical genomics and research. Nature 604: 310-315
Pakos-Zebrucka K, Koryga I, Mnich K, Ljujic M, Samali A, Gorman AM (2016) The integrated stress response. EMBO Rep 17: 1374-1395
Pearce SF, Cipullo M, Chung B, Brierley I, Rorbach J (2021) Mitoribosome Profiling from Human Cell Culture: A High Resolution View of Mitochondrial Translation. Methods Mol Biol 2192: 183-196

Pisarev AV, Hellen CUT, Pestova TV (2007) Recycling of Eukaryotic Posttermination Ribosomal Complexes. Cell 131: 286–299
Poncova K, Wagner S, Jansen ME, Beznoskova P, Gunisova S, Herrmannova A, Zeman J, Dong J, Valasek LS (2019) uS3/Rps3 controls fidelity of translation termination and programmed stop codon readthrough in co-operation with eIF3. Nucleic Acids Res 47: 11326-11343
Pyronnet S, Imataka H, Gingras AC, Fukunaga R, Hunter T, Sonenberg N (1999) Human eukaryotic translation initiation factor 4G (eIF4G) recruits Mnk1 to phosphorylate eIF4E. EMBO Journal 18: 270-279
Rayburn E, Zhang R, He J, Wang H (2005) MDM2 and human malignancies: expression, clinical pathology, prognostic markers, and implications for chemotherapy. Curr Cancer Drug Targets 5: 27-41
Robichaud N, Sonenberg N (2017) Translational control and the cancer cell response to stress. Curr Opin Cell Biol 45: 102-109
Roux PP, Ballif BA, Anjum R, Gygi SP, Blenis J (2004) Tumor-promoting phorbol esters and activated Ras inactivate the tuberous sclerosis tumor suppressor complex via p90 ribosomal S6 kinase. Proc Natl Acad Sci U S A 101: 13489-94
Roux PP, Topisirovic I (2018) Signaling Pathways Involved in the Regulation of mRNA Translation. Mol Cell Biol 38
Ruggero D (2013) Translational control in cancer etiology. Cold Spring Harb Perspect Biol 5
Sayers EW, Bolton EE, Brister JR, Canese K, Chan J, Comeau DC, Connor R, Funk K, Kelly C, Kim S, Madej T, Marchler-Bauer A, Lanczycki C, Lathrop S, Lu Z, Thibaud-Nissen F, Murphy T, Phan L, Skripchenko Y, Tse T et al. (2022) Database resources of the national center for biotechnology information. Nucleic Acids Res 50: D20-D26
Scheper GC, van der Knaap MS, Proud CG (2007) Translation matters: protein synthesis defects in inherited disease. Nat Rev Genet 8: 711-23
She R, Luo J, Weissman JS (2023) Translational fidelity screens in mammalian cells reveal eIF3 and eIF4G2 as regulators of start codon selectivity. Nucleic Acids Res
Shu XE, Mao Y, Jia L, Qian SB (2022) Dynamic eIF3a O-GlcNAcylation controls translation reinitiation during nutrient stress. Nat Chem Biol 18: 134-141
Shuda M, Kondoh N, Tanaka K, Ryo A, Wakatsuki T, Hada A, Goseki N, Igari T, Hatsuse K, Aihara T, Horiuchi S, Shichita M, Yamamoto N, Yamamoto M (2000) Enhanced expression of translation factor mRNAs in hepatocellular carcinoma. Anticancer Res 20: 2489-94
Silvera D, Formenti SC, Schneider RJ (2010) Translational control in cancer. Nat Rev Cancer 10: 254-66
Simonetti A, Guca E, Bochler A, Kuhn L, Hashem Y (2020) Structural Insights into the Mammalian Late-Stage Initiation Complexes. Cell Rep 31: 107497

Smekalova EM, Gerashchenko MV, O'Connor PBF, Whittaker CA, Kauffman KJ, Fefilova AS, Zatsepin TS, Bogorad RL, Baranov PV, Langer R, Gladyshev VN, Anderson DG, Koteliansky V (2020) In Vivo RNAi-Mediated eIF3m Knockdown Affects Ribosome Biogenesis and Transcription but Has Limited Impact on mRNA-Specific Translation. Mol Ther Nucleic Acids 19: 252-266
Sodani K, Patel A, Kathawala RJ, Chen ZS (2012) Multidrug resistance associated proteins in multidrug resistance. Chin J Cancer 31: 58-72
Sonenberg N, Hinnebusch AG (2009) Regulation of Translation Initiation in Eukaryotes: Mechanisms and Biological Targets. Cell 136: 731-745
Spilka R, Ernst C, Mehta AK, Haybaeck J (2013) Eukaryotic translation initiation factors in cancer development and progression. Cancer Lett 340: 9-21
Sriram A, Bohlen J, Teleman AA (2018) Translation acrobatics: how cancer cells exploit alternate modes of translational initiation. EMBO Rep 19
Stokoe D, Macdonald SG, Cadwallader K, Symons M, Hancock JF (1994) Activation of Raf as a result of recruitment to the plasma membrane. Science 264: 1463-7
Tcherkezian J, Cargnello M, Romeo Y, Huttlin EL, Lavoie G, Gygi SP, Roux PP (2014) Proteomic analysis of cap-dependent translation identifies LARP1 as a key regulator of 5'TOP mRNA translation. Genes Dev 28: 357-71
Truitt ML, Ruggero D (2016) New frontiers in translational control of the cancer genome. Nat Rev Cancer 16: 288-304
Tweedie S, Braschi B, Gray K, Jones TEM, Seal RL, Yates B, Bruford EA (2021) Genenames.org: the HGNC and VGNC resources in 2021. Nucleic Acids Res 49: D939-D946
Valášek LS (2012) 'Ribozoomin' – Translation Initiation from the Perspective of the Ribosome-bound Eukaryotic Initiation Factors (eIFs). Curr Protein Pept Sci 13: 305-330
Valasek LS, Zeman J, Wagner S, Beznoskova P, Pavlikova Z, Mohammad MP, Hronova V, Herrmannova A, Hashem Y, Gunisova S (2017) Embraced by eIF3: structural and functional insights into the roles of eIF3 across the translation cycle. Nucleic Acids Res 45: 10948-10968
Wagner S, Bohlen J, Herrmannova A, Jelinek J, Preiss T, Valasek LS, Teleman AA (2022) Selective footprinting of 40S and 80S ribosome subpopulations (Sel-TCP-seq) to study translation and its control. Nat Protoc 17: 2139-2187
Wagner S, Herrmannova A, Hronova V, Gunisova S, Sen ND, Hannan RD, Hinnebusch AG, Shirokikh NE, Preiss T, Valasek LS (2020) Selective Translation Complex Profiling Reveals Staged Initiation and Co-translational Assembly of Initiation Factor Complexes. Mol Cell 79: 546-560 e7
Wagner S, Herrmannova A, Malik R, Peclinovska L, Valasek LS (2014) Functional and Biochemical Characterization of Human Eukaryotic Translation Initiation Factor 3 in Living Cells. Mol Cell Biol 34: 3041-3052

Wagner S, Herrmannova A, Sikrova D, Valasek LS (2016) Human eIF3b and eIF3a serve as the nucleation core for the assembly of eIF3 into two interconnected modules: the yeast-like core and the octamer. Nucleic Acids Res 44: 10772-10788
Wolf DA, Lin Y, Duan H, Cheng Y (2020) eIF-Three to Tango: emerging functions of translation initiation factor eIF3 in protein synthesis and disease. J Mol Cell Biol 12: 403-409
Xia Y, Shen S, Verma IM (2014) NF-kappaB, an active player in human cancers. Cancer Immunol Res 2: 823-30
Xu Z, Hu H, Fang D, Wang J, Zhao K (2021) The deubiquitinase USP38 promotes cell proliferation through stabilizing c-Myc. Int J Biochem Cell Biol 137: 106023
Zhang L, Pan X, Hershey JW (2007) Individual overexpression of five subunits of human translation initiation factor eIF3 promotes malignant transformation of immortal fibroblast cells. J Biol Chem 282: 5790-800
Zhang P, Xiao Z, Wang S, Zhang M, Wei Y, Hang Q, Kim J, Yao F, Rodriguez-Aguayo C, Ton BN, Lee M, Wang Y, Zhou Z, Zeng L, Hu X, Lawhon SE, Siverly AN, Su X, Li J, Xie X et al. (2018) ZRANB1 Is an EZH2 Deubiquitinase and a Potential Therapeutic Target in Breast Cancer. Cell Rep 23: 823-837
Zhang W, Liu HT (2002) MAPK signal pathways in the regulation of cell proliferation in mammalian cells. Cell Res 12: 9-18
Zhang Y, Wang X (2020) Targeting the Wnt/beta-catenin signaling pathway in cancer. J Hematol Oncol 13: 165
Zhao Y, Xiong X, Sun Y (2011) DEPTOR, an mTOR inhibitor, is a physiological substrate of SCF(betaTrCP) E3 ubiquitin ligase and regulates survival and autophagy. Mol Cell 44: 304-16
Zhu P, Li FF, Zeng J, Tang DG, Chen WB, Guo CC (2021) Integrative analysis of the characteristics of lipid metabolism-related genes as prognostic prediction markers for hepatocellular carcinoma. Eur Rev Med Pharmacol Sci 25: 116-126

Figure legends

Figure 1. **Schematic models of the core of MAPK/ERK pathway and human eIF3 complex.** (A) The ERK pathway activation by growth factors and receptor tyrosine kinase. RTKs signals through GRB2-Sos and Ras to activate Raf-Mek-Erk signaling cascade. Active ERK phosphorylates numerous substrates, both nuclear and cytoplasmic, to affect gene transcription, protein translation, cell growth, proliferation and survival. Ras also activates PI3K-AKT pathway that affect cell survival and growth. Conventional PAKs (PAK1-3) phosphorylate and activate c-Raf. Created with Biorender.com. (B) eIF3 subunits forming the PCI/MPN octamer are indicated by the grey background. The rectangle marks the seven α-helices involved in formation of the 7-helix bundle. The Yeast-Like Core (YLC) comprising the eIF3 subunits a, b, g and i is depicted, and so is the eIF3-associated factor eIF3j. Arrows indicate subunits targeted

by siRNA and subjected to Ribo-Seq in this study; eIF3 subcomplexes generated in individual knock-downs are boxed (adapted from (Wagner et al., 2016)).

Figure 2. **Quality control of eIF3e, d, and h knock-downs and the Ribo-Seq data** (A) mRNA levels of the selected downregulated eIF3 subunits were significantly decreased as assessed by quantitative PCR for all replicates. Plot represents the result of all replicates used for RNA-Seq and Ribo-Seq library preparations ± SD. The ddCq value displays the threshold cycle normalized to the reference gene *ALAS1* and to control cells transfected with non-targeting siRNA (NT). The ddCq values are in log2 scale. A ddCq of 0 indicates no change to NT siRNA control; ddCq = 4 indicates a drop to 6.25% (16 fold) compared to NT siRNA control. (B) Downregulation of selected eIF3 subunits targeted by siRNA was determined by Western blotting with GAPDH used as a loading control and antibodies listed in Supplementary Table S3. (C) All Ribo-Seq libraries show typical 3nt periodicity in the CDS. Metagene plots of footprint (FP) length versus 5' end position relative to the first nucleotide (position 0) of start (left) or stop codons (right). The color scale represents FP count as indicated on the right and is plotted in log scale. The labels at the color bar are given in linear scale. Heatmaps are shown for one exemplary replicate from each sample.

Figure 3. **Overview of differential expression analysis.** (A) Principal component analysis of read count per gene of the RNA-Seq and Ribo-Seq libraries. (B - D) Volcano plots of significant ($P_{adjusted} < 0.05$) DTEGs in individual knock-downs: eIF3d^{KD} (B), eIF3e^{KD} (C) and eIF3h^{KD} (D). The volcano plots show the Log2 fold-change of TE (x-axis) *versus* the significance -Log10 p-adjusted value (y-axis). Genes without significant p-adjusted value are plotted in grey, downregulated DTEGs are plotted in blue and upregulated DTEGs in orange. For each plot, the top 10 most significant DTEGs are labeled with gene names. The Volcano plots were generated using modified script from Galaxy (Blankenberg, Von Kuster et al., 2014). (E - G) Venn diagrams depicting the overlap in all DTEGs (E), in downregulated DTEGs (F), and in upregulated DTEGs (G) among eIF3d^{KD}, eIF3e^{KD} and eIF3h^{KD}. Based on the overlaps, DTEGs were divided in several subgroups for further analysis: eIF3d^{KD} "all", eIF3d^{KD} "unique", eIF3e^{KD} "all", eIF3e^{KD} "unique", eIF3d^{KD}/eIF3e^{KD} "common" and eIF3h^{KD} "all".

Figure 4. **KEGG pathway enrichment analysis of the eIF3d^{KD}- and eIF3e^{KD}-associated downregulated DTEGs reveals downregulation of MAPK signaling pathway components.** (A) Venn diagram of the 10 most significantly enriched KEGG pathways for eIF3d^{KD} "all" and eIF3e^{KD} "all" groups of downregulated DTEGs, highlighting that most of the pathways are common to both knock-downs. The MAPK signaling pathway is highlighted in bold. The complete results of the KEGG enrichment analysis with corresponding *p*-values can be found in Supplementary Figure 4. (B) The

list of genes pre-selected for western blot analysis and a heatmap showing their respective log2 fold-change values from differential expression analysis of FP, TE and mRNA in eIF3d^{KD}. Negative values indicating a significant downregulation are in shades of blue, while positive values showing significant upregulation are in shades of orange. NS = not significant p-adjusted value. (C) Western blot analysis of selected proteins constituting the MAPK pathway performed in the indicated knock-downs and the NT control. GAPDH was used as a loading control. This experiment was repeated 3 times with similar results. (D) Western blot analysis of the phosphorylation status of the ERK1/2 proteins (left) and its relative quantification (right), one-sample t-test was used for statistical evaluation, ** = P <0.01, n=2.

Figure 5. **KEGG pathway enrichment analysis of the eIF3d^{KD}- and eIF3e^{KD}-associated upregulated DTEGs reveals upregulation of ribosomal proteins.** (A) Venn diagram of the 10 most significantly enriched KEGG pathways for eIF3d^{KD} "all" and eIF3e^{KD} "all" groups of upregulated DTEGs, highlighting that most of the pathways are common to both knock-downs. Lysosome and Protein processing in ER are highlighted in bold. The complete results of the KEGG enrichment analysis with corresponding *p*-values can be found in Supplementary Figure 7. (B) Venn diagram as in A but displaying eIF3d^{KD} "translation only" and eIF3e^{KD} "translation only" groups of the upregulated DTEGs. (C) The bar chart shows the top 10 enriched KEGG terms for eIF3e^{KD} unique upregulated DTEGs. Orange bars correspond to terms with significant *p*-values (< 0.05), grey bars correspond to terms with not significant *p*-values (> 0.05). The *p*-values were calculated by Enrichr gene set search engine. (D) The list of genes pre-selected for western blot analysis and a heatmap showing their respective log2 fold-change values from differential expression analysis of FP, TE and mRNA in eIF3e^{KD} and eIF3d^{KD}. Positive values indicating significant upregulation are in shades of orange. NS = not significant p-adjusted value. (E) Western blot analysis of selected ribosomal proteins performed in the indicated knock-downs and the NT control. GAPDH was used as a loading control. This experiment was repeated 3 times with similar results.

Figure 6. **KEGG pathway and GO enrichment analysis of the eIF3h^{KD}-associated DTEGs reveals downregulation of proto-oncogene MDM2 and a defective stress-induced upregulation of ATF4.** (A) The bar chart shows the top 10 enriched KEGG terms for eIF3h^{KD} "all downregulated" DTEGs. Blue bars correspond to terms with significant *p*-values (< 0.05), grey bars correspond to terms with not significant *p*-values (> 0.05). The *p*-values were calculated by Enrichr gene set search engine. (B) The bar chart shows the top 10 enriched GO Biological Process terms for eIF3h^{KD} "all downregulated" DTEGs. Blue bars correspond to terms with significant *p*-values (< 0.05). The *p*-values were calculated by Enrichr gene set search engine. PCP; protein catabolic process. (C) Western blot analysis of the MDM2 expression preformed in the

indicated knock-downs and NT control. GAPDH was used as a loading control. (D) Western blot analysis of the stress-induced upregulation of ATF4 expression performed in the indicated knock-downs and NT control. Before harvesting, cells were incubated for 3 hours with 1mM Thapsigargin to induce ER stress or with DMSO as a stress-free control. GAPDH was used as a loading control.

Figure 7. **Differential TE transcripts in eIF3d^{KD} and eIF3e^{KD} show negative correlation with the UTR length while they positively correlate with GC content of their 3' UTRs and CDSes.** (A) Bar plot showing the Spearman correlation between the observed ΔTE values for all genes with assigned adjusted *p*-values in each knock-down and different mRNA features (5' and 3' UTR length or GC content, uORF content in 5' UTR). *** = P < 10^{-20}, ** = P < 10^{-10}, * = P < 0.005. (B-C) Box and whisker plots comparing UTR lengths or GC content (in UTRs or CDS) among mRNAs with TE significantly increased (red, upregulated), decreased (blue, downregulated), or unchanged (white) in eIF3d^{KD} (B) and eIF3e^{KD} (C); *** = Padj < 10^{-10} , ** = Padj < 10^{-5}, * = Padj < 0.05, color indicates comparison set. (D) Same as in (B-C) but for the number of AUG-initiated uORFs in 5' UTRs in the eIF3d, eIF3e and eIF3h knock-downs. Outliers are not shown for better clarity. (E) Histogram of the frequency of AUG-initiated uORFs per 5' UTR in all transcripts listed in the uORFdb database that were assigned a *p*-value in this study (n=11450), for downregulated translation only DTEGs in eIF3d^{KD} (n=1027) and for downregulated translation only DTEGs in eIF3e^{KD} (n=618). (F) Venn diagram of the overlap between eIF3d/e^{KD} DTEGs and mRNAs directly interacting with eIF3 as determined by the CLIP assay in (Lee et al., 2015). (G) Venn diagram summarizing the main results of this study. Groups of significant DTEGs identified in given knock-downs (encircled – color-coded) are indicated by a blue arrow for downregulated or an orange arrow for upregulated. Results confirmed by western blotting are shown in bold. Ribosomal proteins were placed on the borderline between eIF3d^{KD} and eIF3e^{KD} because they were identified as eIF3e^{KD} "unique upregulated" DTEGs, but their protein levels were elevated in both eIF3e^{KD} and eIF3d^{KD}, as shown by western blotting. The "MAPK/ERK signaling" is shown in bold italics because it is an independent phenomenon that could be detected only by western blotting.

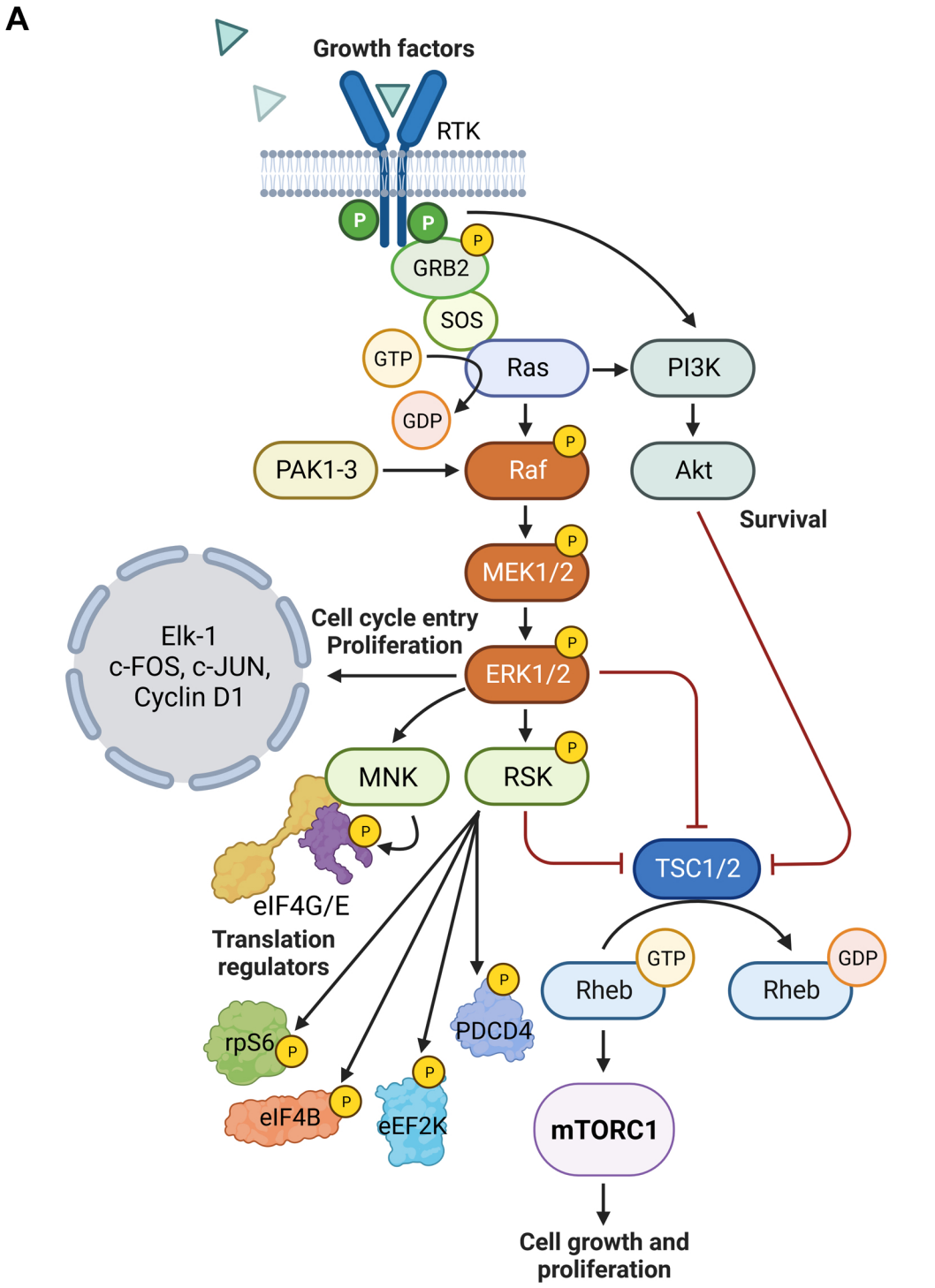
A
Growth factors
RTK
P
P
P
GRB2
SOS
GTP
Ras
PI3K
GDP
PAK1-3
Raf
Akt
Survival
MEK1/2
Elk-1
c-FOS, c-JUN,
Cyclin D1
Cell cycle entry
Proliferation
ERK1/2
MNK
RSK
eIF4G/E
Translation
regulators
TSC1/2
GTP
GDP
Rheb
Rheb
rpS6
PDCD4
eIF4B
eEF2K
mTORC1
Cell growth and
proliferation

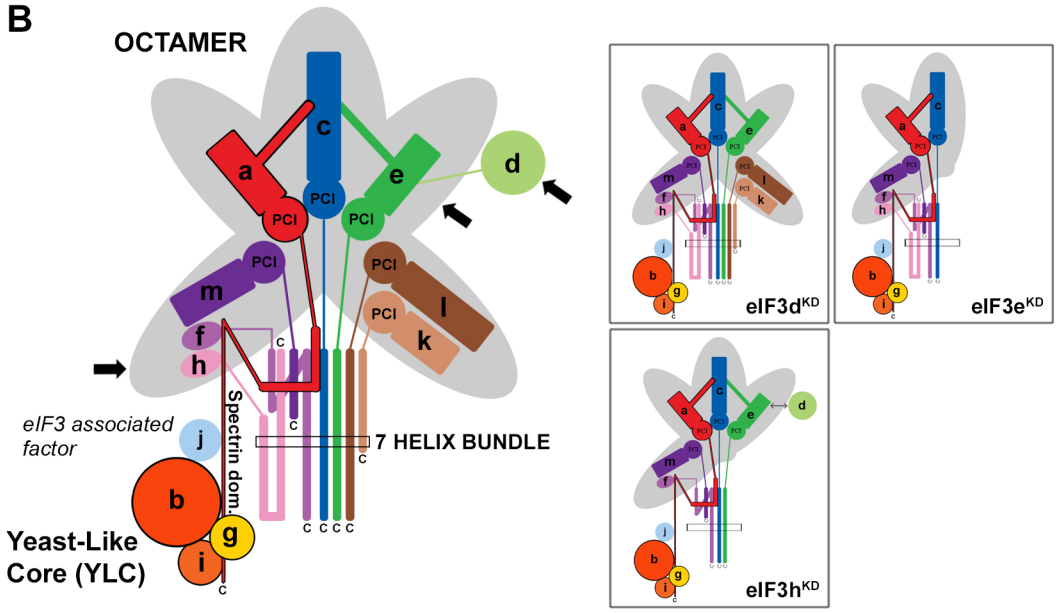
B
OCTAMER
a
b
c
d
e
f
g
h
i
j
k
l
m
PCI
eIF3 associated
factor
Spectrin dom.
7 HELIX BUNDLE
Yeast-Like
Core (YLC)
eIF3d^KD
eIF3e^KD
eIF3h^KD

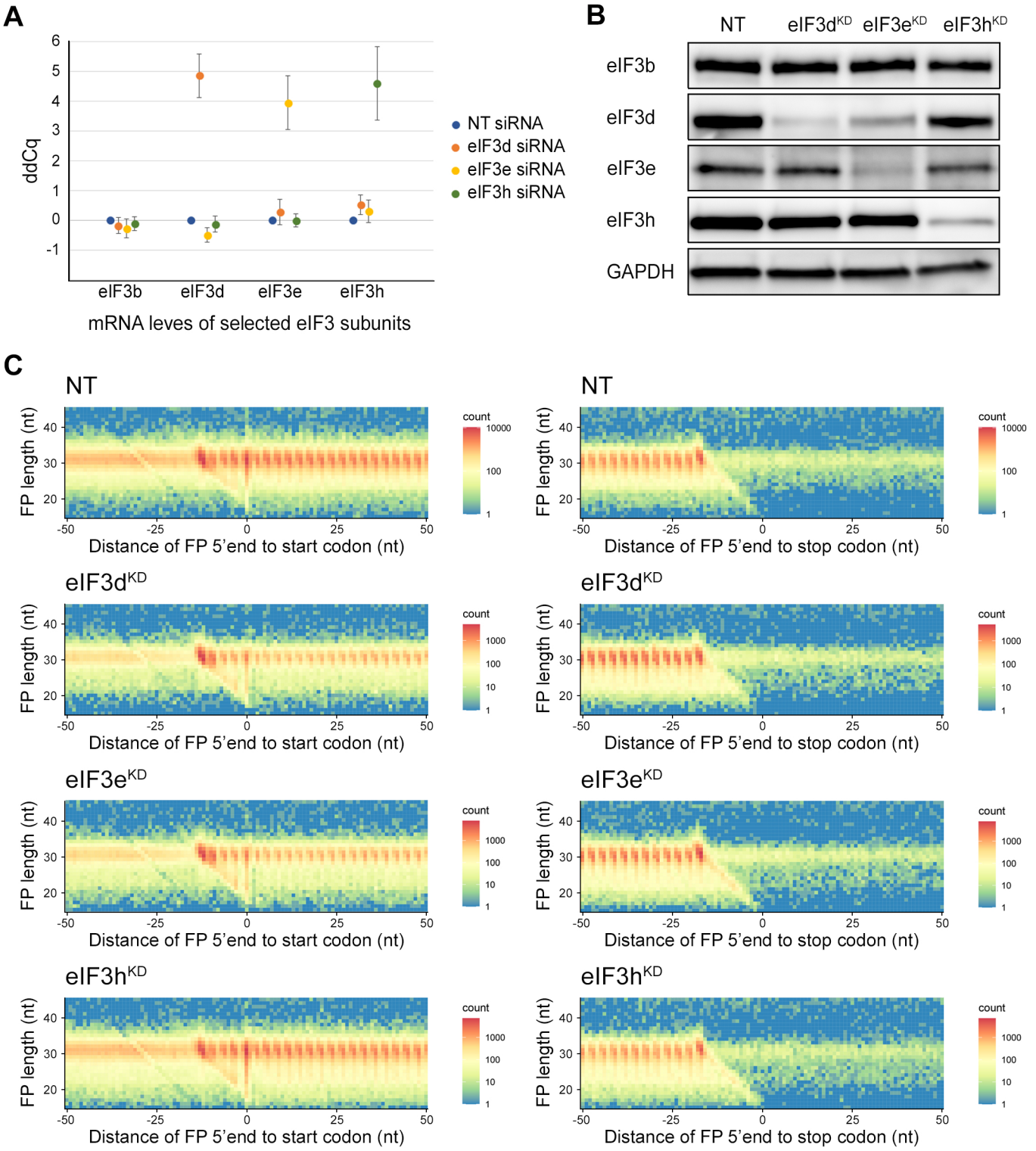
A
ddCq
6
5
4
3
2
1
0
-1
eIF3b
eIF3d
eIF3e
eIF3h
mRNA leves of selected eIF3 subunits
NT siRNA
eIF3d siRNA
eIF3e siRNA
eIF3h siRNA
B
NT
eIF3d^KD
eIF3e^KD
eIF3h^KD
eIF3b
eIF3d
eIF3e
eIF3h
GAPDH
C
NT
eIF3d^KD
eIF3e^KD
eIF3h^KD
FP length (nt)
Distance of FP 5'end to start codon (nt)
Distance of FP 5'end to stop codon (nt)
count
10000
1000
100
10
1
-50
-25
0
25
50
20
30
40

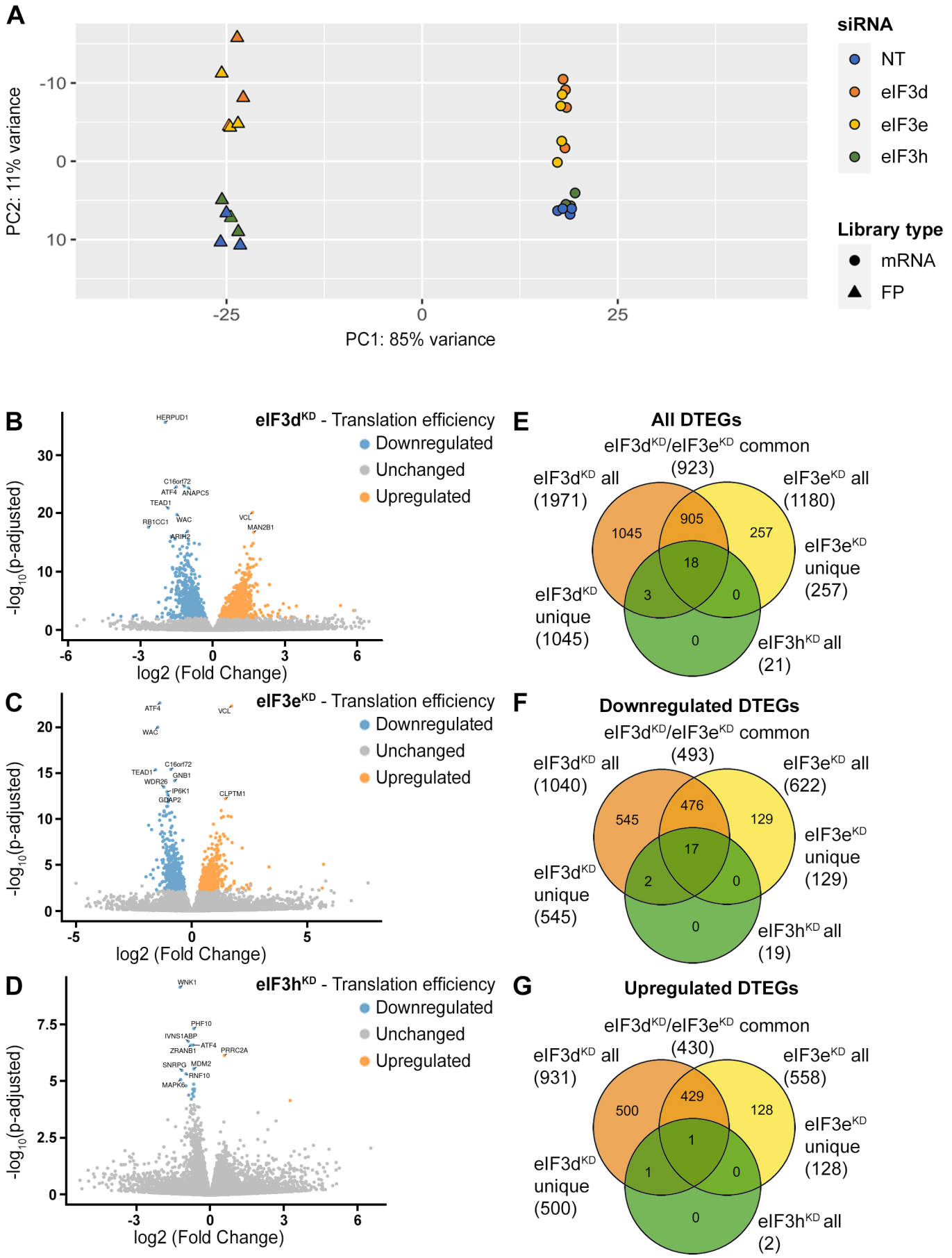
A
PC2: 11% variance
PC1: 85% variance
siRNA
NT
eIF3d
eIF3e
eIF3h
Library type
mRNA
FP
B
eIF3d^KD - Translation efficiency
Downregulated
Unchanged
Upregulated
-log10(p-adjusted)
log2 (Fold Change)
HERPUD1
C16orf72
ATF4
ANAPC5
TEAD1
RB1CC1
WAC
ARIH2
VCL
MAN2B1
C
eIF3e^KD - Translation efficiency
ATF4
VCL
WAC
TEAD1
C16orf72
GNB1
WDR26
IP6K1
GDAP2
CLPTM1
D
eIF3h^KD - Translation efficiency
WNK1
PHF10
IVNS1ABP
ATF4
ZRANB1
PRRC2A
SNRPG
MDM2
RNF10
MAPK6
E
All DTEGs
eIF3d^KD/eIF3e^KD common (923)
eIF3d^KD all (1971)
eIF3e^KD all (1180)
eIF3e^KD unique (257)
eIF3d^KD unique (1045)
eIF3h^KD all (21)
1045
905
257
18
3
0
0
F
Downregulated DTEGs
eIF3d^KD/eIF3e^KD common (493)
eIF3d^KD all (1040)
eIF3e^KD all (622)
eIF3e^KD unique (129)
eIF3d^KD unique (545)
eIF3h^KD all (19)
545
476
129
17
2
0
0
G
Upregulated DTEGs
eIF3d^KD/eIF3e^KD common (430)
eIF3d^KD all (931)
eIF3e^KD all (558)
eIF3e^KD unique (128)
eIF3d^KD unique (500)
eIF3h^KD all (2)
500
429
128
1
1
0
0

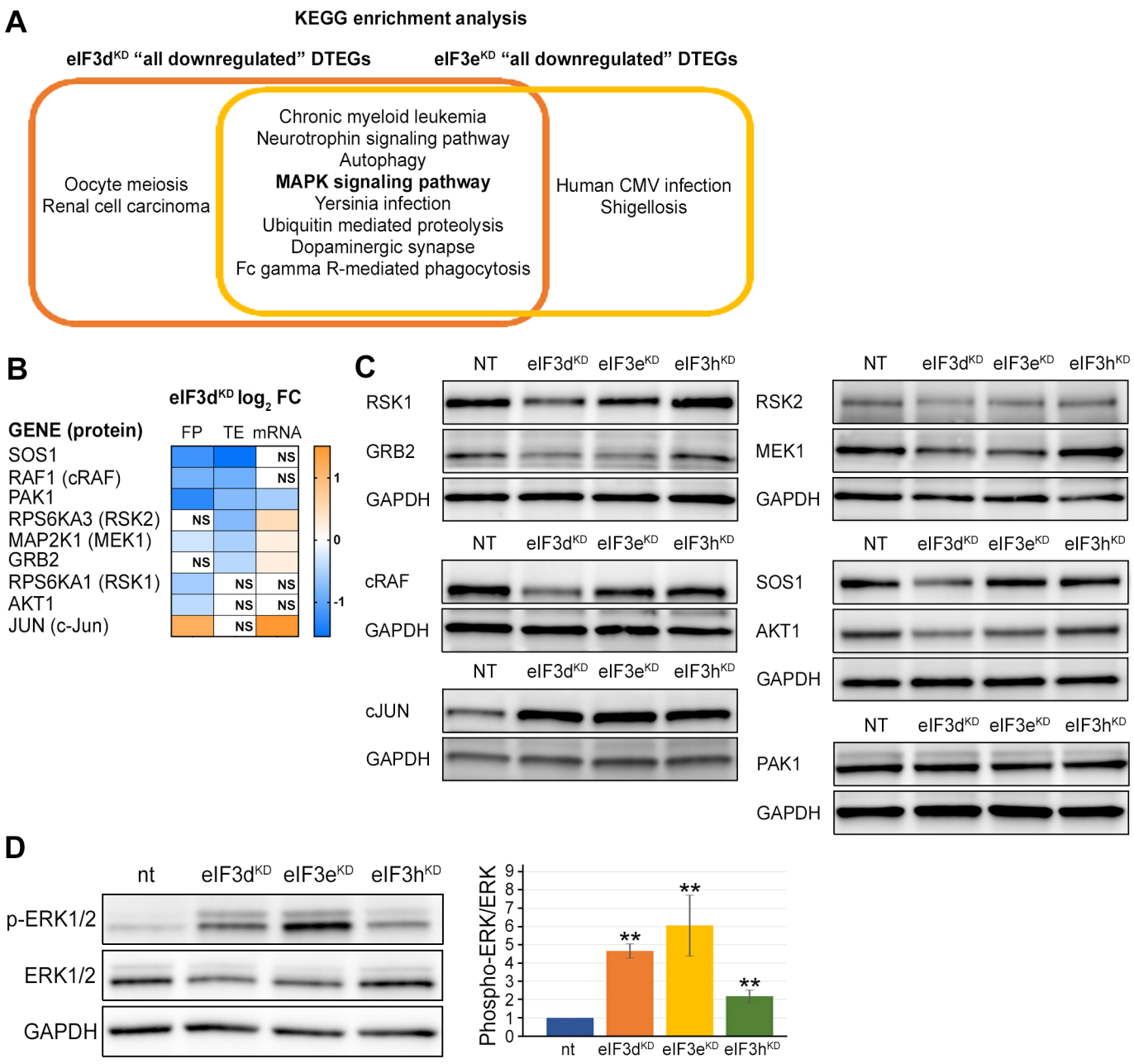
A
KEGG enrichment analysis
eIF3d^KD "all downregulated" DTEGs
eIF3e^KD "all downregulated" DTEGs
Oocyte meiosis
Renal cell carcinoma
Chronic myeloid leukemia
Neurotrophin signaling pathway
Autophagy
MAPK signaling pathway
Yersinia infection
Ubiquitin mediated proteolysis
Dopaminergic synapse
Fc gamma R-mediated phagocytosis
Human CMV infection
Shigellosis
B
eIF3d^KD log2 FC
GENE (protein)
FP
TE
mRNA
SOS1
RAF1 (cRAF)
PAK1
RPS6KA3 (RSK2)
MAP2K1 (MEK1)
GRB2
RPS6KA1 (RSK1)
AKT1
JUN (c-Jun)
NS
1
0
-1
C
NT
eIF3d^KD
eIF3e^KD
eIF3h^KD
RSK1
GRB2
GAPDH
RSK2
MEK1
cRAF
SOS1
AKT1
cJUN
PAK1
D
nt
p-ERK1/2
ERK1/2
Phospho-ERK/ERK
**

A KEGG enrichment analysis

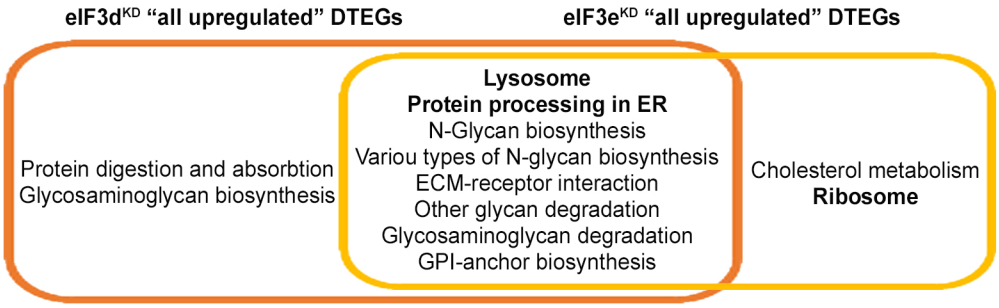

B

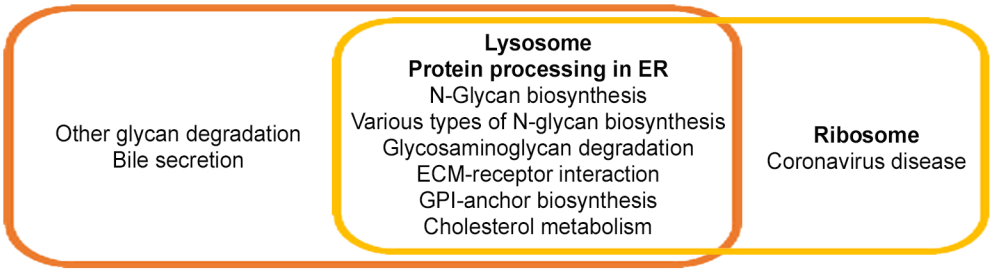

C eIF3e^KD unique upregulated DTEGs

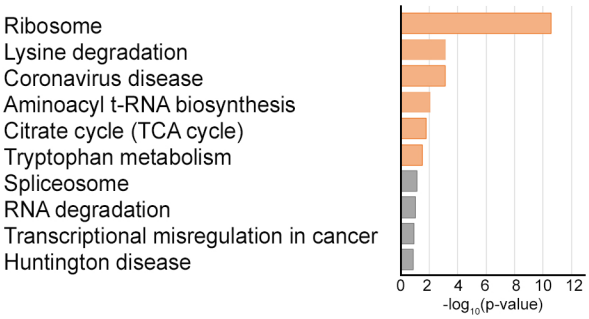

D

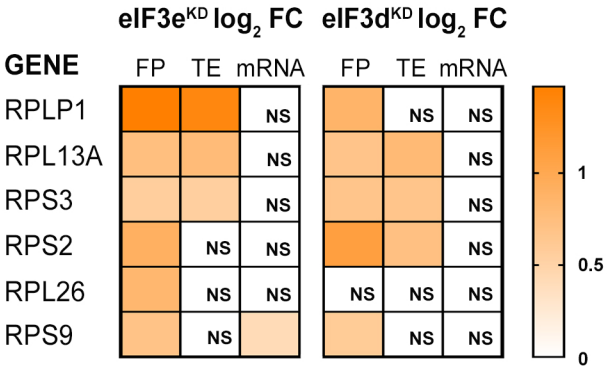

E

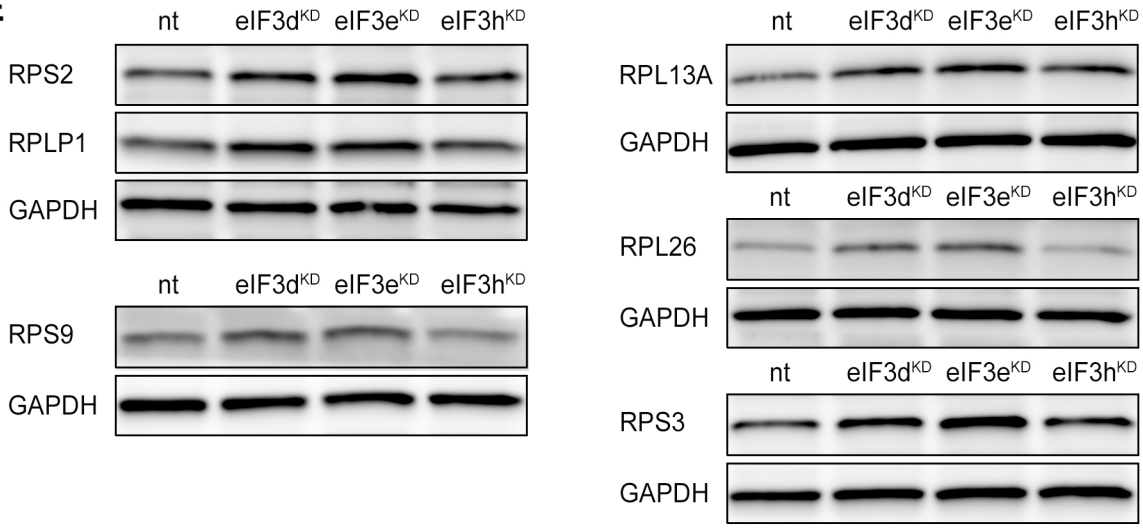

A **eIF3h^{KD} "all downregulated" DTEGs**

KEGG enrichment analysis

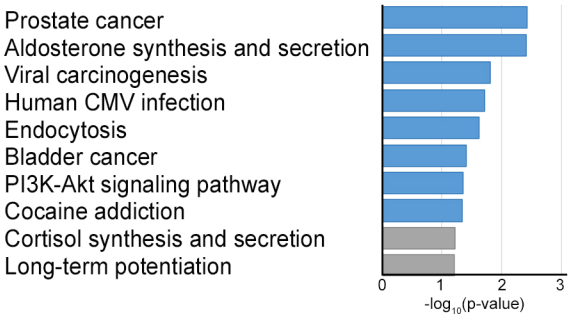

B **eIF3h^{KD} all downregulated DTEGs**

GO biological process enrichment analysis

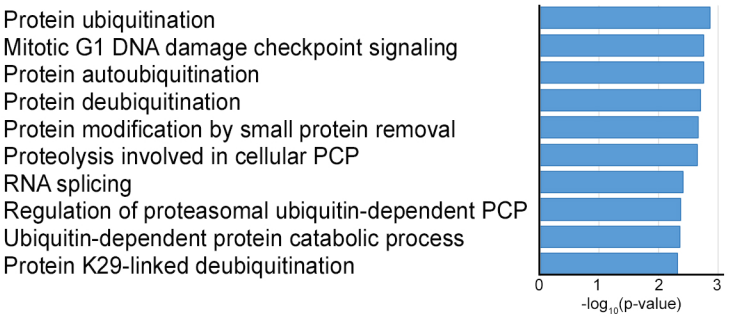

C

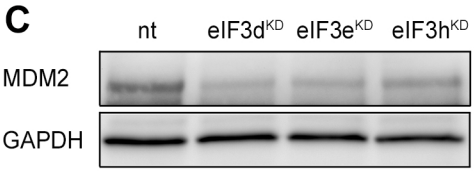

D

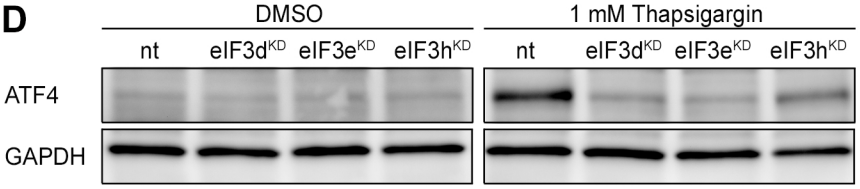

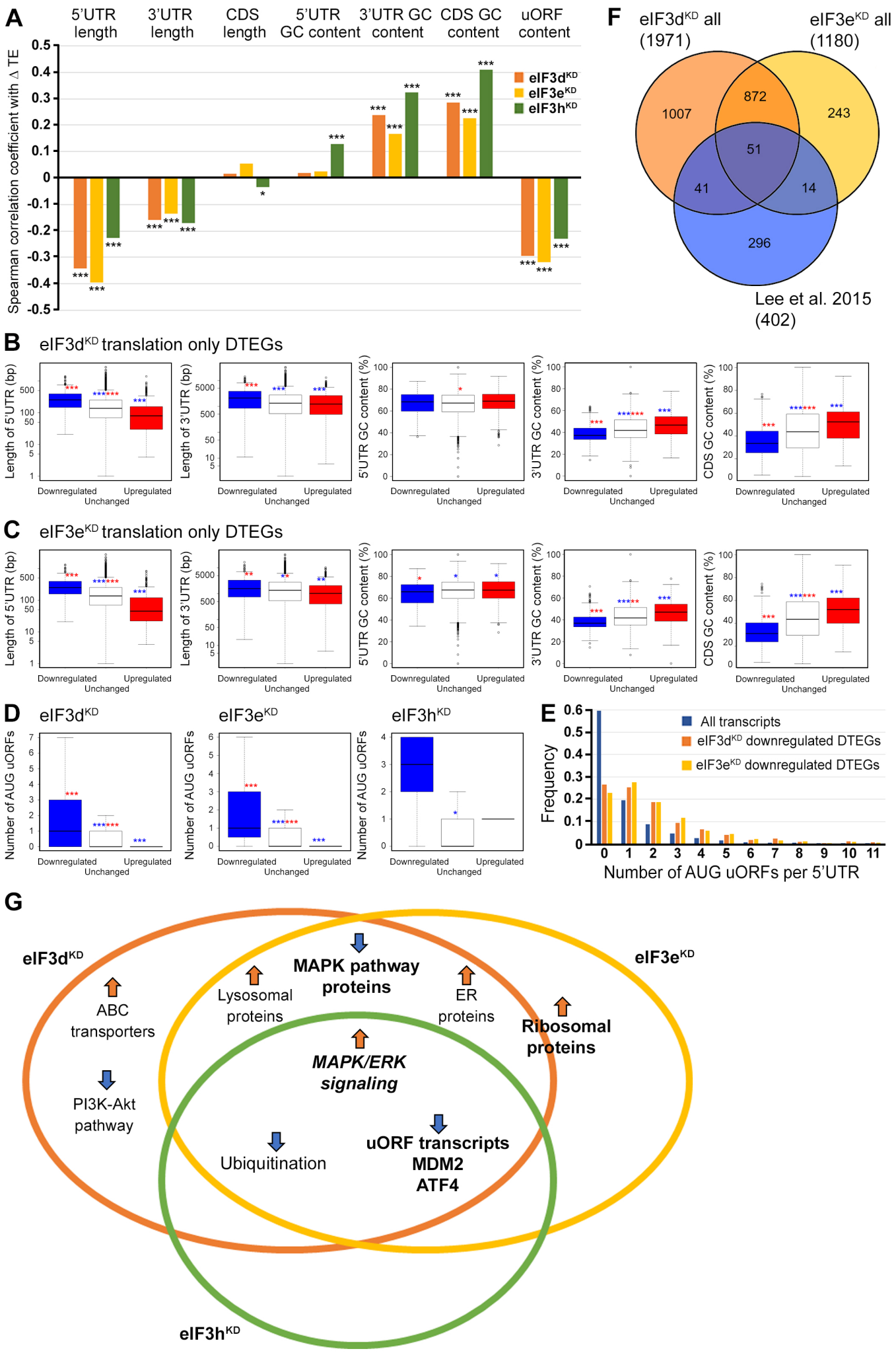
A
5'UTR length
3'UTR length
CDS length
5'UTR GC content
3'UTR GC content
CDS GC content
uORF content
Spearman correlation coefficient with Δ TE
eIF3d^KD
eIF3e^KD
eIF3h^KD
F
eIF3d^KD all (1971)
eIF3e^KD all (1180)
Lee et al. 2015 (402)
1007
872
243
51
41
14
296
B
eIF3d^KD translation only DTEGs
Length of 5'UTR (bp)
Length of 3'UTR (bp)
5'UTR GC content (%)
3'UTR GC content (%)
CDS GC content (%)
Downregulated
Unchanged
Upregulated
C
eIF3e^KD translation only DTEGs
D
eIF3d^KD
eIF3e^KD
eIF3h^KD
Number of AUG uORFs
E
All transcripts
eIF3d^KD downregulated DTEGs
eIF3e^KD downregulated DTEGs
Frequency
Number of AUG uORFs per 5'UTR
G
eIF3d^KD
eIF3e^KD
eIF3h^KD
ABC transporters
PI3K-Akt pathway
Lysosomal proteins
MAPK pathway proteins
ER proteins
Ribosomal proteins
MAPK/ERK signaling
Ubiquitination
uORF transcripts
MDM2
ATF4